

Journal of Print and Media Technology Research

Scientific contributions

Nonlinear behavior in electrical properties
of fully screen printed electroluminescent panels

*Katrin Hirmer, Christina Bodenstein,
Hans Martin Sauer, Edgar Dörsam and Klaus Hofmann*

145

An approach to risk-based maintenance strategy
of a printing press

Avijit Kar and Arun Kiran Pal

155

The starch addition to a curtain coating formulation
and its effect on pitting

*Samantha L. Schoenfelder, Alexandra Pekarovicova
and Paul D. Fleming*

167

ISSN 2414-6250



9 772414 625001

Editor-in-Chief

Published by **iarigai**
www.iarigai.org

Gorazd Golob (Ljubljana)

The International Association of Research
Organizations for the Information, Media
and Graphic Arts Industries

Journal of Print and Media Technology Research

A PEER-REVIEWED QUARTERLY

PUBLISHED BY

The International Association of Research Organizations
for the Information, Media and Graphic Arts Industries
Magdalenenstrasse 2, D-64288 Darmstadt, Germany
<http://www.iarigai.org>
journal@iarigai.org

EDITORIAL BOARD

EDITOR-IN-CHIEF

Gorazd Golob (Ljubljana, Slovenia)

EDITORS

Timothy C. Claypole (Swansea, UK)
Edgar Dörsam (Darmstadt, Germany)
Nils Enlund (Helsinki, Finland)
Mladen Lovreček (Zagreb, Croatia)
Renke Wilken (Munich, Germany)
Scott Williams (Rochester, USA)

ASSOCIATE EDITOR

Markéta Držková (Pardubice, Czech Republic)

SCIENTIFIC ADVISORY BOARD

Darko Agić (Zagreb, Croatia)
Anne Blayo (Grenoble, France)
Wolfgang Faigle (Stuttgart, Germany)
Elena Fedorovskaya (Rochester, USA)
Patrick Gane (Helsinki, Finland)
Diana Gregor Svetec (Ljubljana, Slovenia)
Jon Yngve Hardeberg (Gjøvik, Norway)
Ulrike Herzau Gerhardt (Leipzig, Germany)
Gunter Hübner (Stuttgart, Germany)
Marie Kaplanová (Pardubice, Czech Republic)
John Kettle (Espoo, Finland)
Helmut Kipphan (Schwetzingen, Germany)
Björn Kruse (Linköping, Sweden)
Yuri Kuznetsov (St. Petersburg, Russian Federation)
Magnus Lestelius (Karlstad, Sweden)
Patrice Mangin (Trois Rivières, Canada)
Thomas Mejtoft (Umeå, Sweden)
Erzsébet Novotny (Budapest, Hungary)
Anastasios Politis (Athens, Greece)
Anu Seisto (Espoo, Finland)
Johan Stenberg (Stockholm, Sweden)
Philipp Urban (Darmstadt, Germany)

A mission statement

To meet the need for a high quality scientific publishing platform in its field, the International Association of Research Organizations for the Information, Media and Graphic Arts Industries is publishing a quarterly peer-reviewed research journal.

The journal is fostering multidisciplinary research and scholarly discussion on scientific and technical issues in the field of graphic arts and media communication, thereby advancing scientific research, knowledge creation, and industry development. Its aim is to be the leading international scientific journal in the field, offering publishing opportunities and serving as a forum for knowledge exchange between all those interested in contributing to or learning from research in this field.

By regularly publishing peer-reviewed, high quality research articles, position papers, surveys, and case studies as well as review articles and topical communications, the journal is promoting original research, international collaboration, and the exchange of ideas and know-how. It also provides a multidisciplinary discussion on research issues within the field and on the effects of new scientific and technical developments on society, industry, and the individual. Thus, it intends to serve the entire research community as well as the global graphic arts and media industry.

The journal is covering fundamental and applied aspects of at least, but not limited to, the following topics:

Printing technology and related processes

- ⊕ Conventional and special printing
- ⊕ Packaging
- ⊕ Fuel cells and other printed functionality
- ⊕ Printing on biomaterials
- ⊕ Textile and fabric printing
- ⊕ Printed decorations
- ⊕ Materials science
- ⊕ Process control

Premedia technology and processes

- ⊕ Colour reproduction and colour management
- ⊕ Image and reproduction quality
- ⊕ Image carriers (physical and virtual)
- ⊕ Workflow and management

Emerging media and future trends

- ⊕ Media industry developments
- ⊕ Developing media communications value systems
- ⊕ Online and mobile media development
- ⊕ Cross-media publishing

Social impact

- ⊕ Media in a sustainable society
- ⊕ Environmental issues and sustainability
- ⊕ Consumer perception and media use
- ⊕ Social trends and their impact on media

Submissions to the Journal

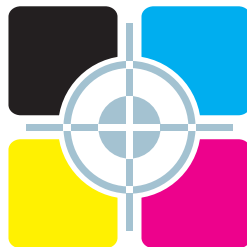
Submissions are invited at any time and, if meeting the criteria for publication, will be rapidly submitted to peer-review and carefully evaluated, selected and edited. Once accepted and edited, the papers will be published as soon as possible.

✉ Contact the Editorial office: journal@iarigai.org

Journal of Print and Media Technology Research

3-2019

September 2019



The information published in this journal is obtained from sources believed to be reliable and the sole responsibility on the contents of the published papers lies with their authors. The publishers can accept no legal liability for the contents of the papers, nor for any information contained therein, nor for conclusions drawn by any party from it.

Journal of Print and Media Technology Research is listed in:

Emerging Sources Citation Index

Scopus

Index Copernicus International

PiraBase (by Smithers Pira)

Paperbase (by Innventia and Centre Technique du Papier)

NSD – Norwegian Register for Scientific Journals, Series and Publishers

Contents

A letter from the Editor
Gorazd Golob 143

Scientific contributions

Nonlinear behavior in electrical properties
of fully screen printed electroluminescent panels
*Katrin Hirmer, Christina Bodenstein,
Hans Martin Sauer, Edgar Dörsam and Klaus Hofmann* 145

An approach to risk-based maintenance strategy
of a printing press
Avijit Kar and Arun Kiran Pal 155

The starch addition to a curtain coating formulation
and its effect on pitting
*Samantha L. Schoenfelder, Alexandra Pekarovicova
and Paul D. Fleming* 167

Topicalities

Edited by Markéta Držková

News & more 179
Bookshelf 181
Events 187



A letter from the Editor

Gorazd Golob

Editor-in-Chief

E-mail: gorazd.golob@jpmtr.org
journal@iarigai.org

The final editing and production of the September issue of the Journal were done during and immediately after the International Research Conference of *iarigai* in Stuttgart. We are still under the impression of many interesting and quality presentations, and now we are expecting new papers for publication in the Journal.

In the present issue, the original scientific paper on the nonlinearity of screen printed electroluminescent panels stands out among the three articles. By measuring the properties of electroluminescent panels under different conditions, especially at low and high voltages, and in dark and light environment, the authors explain their operation and also open up new possibilities in the study of optical and radiation sensors. The second paper deals with the more traditional area of maintenance strategy of a printing press, where we can improve the knowledge and risk management of the installed equipment in the print house, by the implementation of an appropriate approach. In the third article, the authors present a study of the effect of starch addition in the paper coating formulation on the pitting, which has a significant effect on the surface of coated paper and thus on the quality of the print.

The editor Markéta Držková (marketa.drzkova@jpmtr.org) in the Topicalities of this issue prepared an overview of the new and updated ISO standards, and short info on the results of the survey on system integration – one of the expected topics at Drupa 2020.

Among the new books, she reviewed new publications, among which there is highlighted book on multisensory packaging, and introduction of new and partly refurbished work – a series of 26 books in the field of digital and print media design. Although it is in German, some of the contents of the same authors have already been published in English in the past, so we can hope that this set of textbooks and workbooks will also be available in English in the future and thus used in the wider international area.

The three doctoral theses selected differ in content as well as geographically, thus providing insight into the breadth of the research area we identify with.

Robert Wiesenberger successfully defended his thesis at Columbia University, New York, USA. He researched and presented the life and work of Muriel Ruth Cooper, who worked as a graphic designer, educator and researcher at MIT, as well as her grandness and impact on major turning points in the press and media design in the twentieth century.

Mima Kurian defended her doctoral thesis on 3D printed bone-like composites at Victoria University of Wellington, New Zealand. Using the appropriate material based on chitosan and calcium carbonate, she produced 3D structures with a nano and macro-pores using synthetic biomineralization method, resulting in material comparable to the bone and tested its properties.

At Karlstad University, Sweden, Sofia Thorman defended her doctoral thesis in the field of absorption and distribution of ink in flexography. She investigated the interactions of printing ink with the base substrate as well as with the previously printed surface in flexography and related causes of print non-uniformity. She has also tested the new staining method in other fields and has proven its usefulness for determining water-moisture interference in lithographic offset printing.

Announced changes to the Journals editorial team are already underway, though they have not yet been finally adopted and implemented. You are invited to take the opportunity to publish the results of your research work in the Journal. The call for papers is constantly open. We would also appreciate your tips on interesting events, new books or theses from the fields covered by the Journal, aimed at **iarigai** members, subscribers to the Journal and all other experts reading and using it as a reference in their research activities.

Ljubljana, September 2019

JPMTR 125 | 1905
DOI 10.14622/JPMTR-1905
UDC 655.1:537.5/530.1

Original scientific paper
Received: 2019-03-07
Accepted: 2019-09-15

Nonlinear behavior in electrical properties of fully screen printed electroluminescent panels

Katrin Hirmer¹, Christina Bodenstein², Hans Martin Sauer², Edgar Dörsam² and Klaus Hofmann¹

¹Technische Universität Darmstadt,
Integrated Electronic Systems Lab,
Merckstraße 25, 64283 Darmstadt, Germany

²Technische Universität Darmstadt,
Institute of Printing Science and Technology,
Magdalenenstr. 2, 64289 Darmstadt, Germany

katrin.hirmer@ies.tu-darmstadt.de
bodenstein@idd.tu-darmstadt.de
sauer@idd.tu-darmstadt.de
doersam@idd.tu-darmstadt.de
klaus.hofmann@ies.tu-darmstadt.de

Abstract

We study the influences of printing parameters of fully screen printed electroluminescent panels on frequency and voltage dependent electrical properties of these devices. Significant nonlinear electrical features as well as a sensitivity to external illumination were observed. By varying the number of subsequent wet-in-wet printing steps within the dielectric and the luminescent layers of the electroluminescent panel, we studied the capacitive and dissipative behavior of current transport in the device. We used a novel method of high voltage impedance spectroscopy at frequencies between 10 Hz and 1 MHz with voltages up to 70 V_{rms} and compared measurements taken in dark and illuminated ambiances. We propose a qualitative model on the nonlinearity based on ferroelectric and semiconductive features of the dielectric layers as described by the Drude model.

Keywords: printed electronics, printing parameters, high voltage impedance spectroscopy, AC powder electroluminescence, electroluminescent panel characterization

1. Introduction

Electroluminescent (EL) lighting technology is based on light emission from a luminescent material which is exposed to an alternating electric field. It is a non-thermal source of light which can be printed with a very low height. The EL panels are commonly produced by continuous coating techniques (Ranfeld, 2010). However, printing technology enables the efficient reproduction of structured layers by transferring a fluid from a printing form to a substrate with the advantage of printing specific structures in a cost-effective way.

In graphical printing technology, images are generated by superposition of dots with distinct primary colors (CMYK). The so-called raster dots must be small enough to create the impression of a continuous color. Thus, the focus in graphical printing is the color perception of the human eye. In contrast, the focus in printed electronics is on electrical properties, layer thickness and surface quality. The materials used for printed electronics are, for example, polymers, conduc-

tive or insulating materials which have to be printed continuously. Printed EL panels have already been created by screen printing (Sauer, Ranfeld, and Dörsam, 2010), flexographic printing (Ranfeld, Theopold and Dörsam, 2011), and pad printing technology (Lee, et al., 2010; Bodenstein, et al., 2018).

Compared to graphical printing, functional printing requires electrical characterization of the devices. Relations between printing parameters and electrical properties are of great interest to design the devices with respect to their electrical behavior. This paper focuses on the characterization of fully screen printed EL panels and draws conclusions to the printing parameters of the layer.

The paper is organized as follows: Section 2 explains the materials and methods which were used to print the EL samples. The printed panels are electrically characterized in Section 3. Section 4 discusses the findings of Section 3 and draws conclusions to the printing process. The overall paper is concluded in Section 5.

2. Printing process and materials

The EL panel is printed using the layer stack shown in Figure 1, starting with the electric rear electrode. As a substrate, we used PET, Hostaphan GN 4600 from Pütz Folien. Each layer requires material with specific properties, for example conductivity and transparency for the front electrode or isolating properties for the insulating layer. Each layer is printed, partially in several subsequent deposition steps and then dried before the next layer is printed on top of it.

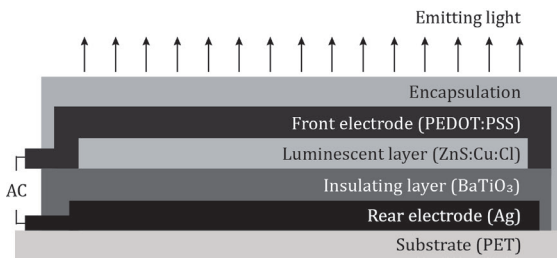


Figure 1: Schematic layer structure of the printed electroluminescent panels

Samples in other publications were partially screen printed onto a conductive precoated material or fabricated by spin coating or vacuum deposition (Kaiser, Marques and Correa, 2013; Kim, et al., 2011; Adachi, et al., 1988). The EL panels in this study were manufactured entirely by screen printing, using a semi-automatic flat screen printing machine K15Q SL from KBA Kammann GmbH.

In the present study, we used printing inks and materials, which could be physically (thermally) or chemically (UV) cured. The advantage of UV curable materials is the low, almost negligible shrinkage in the curing process, and a fast-continuing processing compared to solvent based ink.

For later validation of the electrical parameters, we considered two different EL panel sizes, 16 cm² and 4 cm² of the luminescent area, each disk and square shaped. Processing parameters were identical since all four layouts were printed in the same printing run. We used commercially available screen printing UV inks for the insulating and the luminescent layer. For the former, the ink consists of ferroelectric BaTiO₃ particles dispersed in a varnish, with a solid content of 50 %. As the luminescent layer, zinc sulfide ZnS:Cu:Cl particles were processed in a widely used UV binder and optimized for screen printing. A solvent-based material was used for the rear electrode, whereas the transparent front electrode was made using an aqueous dispersion. A thermal curing process of 20 min. was necessary for drying the electrode material.

Meshes with a stencil thickness of 8–12 μm of emulsion over the mesh, and a mesh cover angle of 22.5° were used. Printing and drying were done at approximately 23 °C at 50 % relative humidity. The hot air oven (HAO) used for drying, took its air inflow from this atmosphere as well, with an air exhaust flow of 140 m³h⁻¹. The used printing inks and related screen parameters are listed in Table 1.

Table 1: Processing materials used for screen printed electroluminescent samples

Layer	Material (ink)	Mesh material	Mesh count [1/cm]	Mesh thread diameter [μm]
Rear electrode	Ag (Electrodag PF050)	metal	95	36
Insulating layer	BaTiO ₃ (Elantas EL7030)	polyester	64	64
Luminescent layer	ZnS:Cu:Cl (Elantas 7001)	polyester	100	40
Front electrode	PEDOT:PSS (EasyCon P3145)	polyester	140	34
Encapsulation	Dupont encapsulant	polyester	100	40

Table 2: Processing parameters used for screen printed electroluminescent samples

Layer	Printing velocity [m/s]	Squeegee hardness [Shore A]	Drying conditions	# Printing steps	
				Batch 1	Batch 2
Rear electrode	0.4	55	HAO: 120 °C 20 min	1	1
Insulating layer	0.4	75	UV: 70 % 15 m/min	1–4	2
Luminescent layer	0.1	75	UV: 70 % 15 m/min	2	1–4
Front electrode	1.0	75	HAO: 100 °C 20 min	3	3
Encapsulation	0.3	65	HAO: 100 °C 20 min	2	2

The processing parameters such as printing velocity, squeegee hardness, drying conditions and the number of repeated printing steps, which were used for specific layers, are listed in Table 2. They largely follow the recommendations of the manufacturer and proved to be satisfactory for defect-free printing.

The dielectric and the luminescent layers were built up by a sequence of several subsequent printing steps. The ink of each subsequent step was printed on the preceding layer before it had solidified, i.e. layer deposition consisted of multiple wet-in-wet steps. Subsequently, the layer was dried according to Table 2. In this way, we created panels with different insulating and luminescent layer thicknesses and thus distinct electrical properties.

For studying the influence of the insulating layer thickness, we varied the number of wet-in-wet printing steps of the insulating material from one to four using two printing steps for the luminescent layer (Batch 1). In order to study the influence of the luminescent layer thickness, the number of printing steps was defined analogously for the respective layers (Batch 2).

Also here, the subsequent steps were deposited without intermediate drying. Both insulating and luminescent layers were cured in a drying conveyor oven system by IST with UV radiation spectrum of 180–450 nm. The curing power was set to 70 % of the nominal maximal power of 8.0 kW. Finally, an encapsulation layer was added for insulation and protection against air and humidity, using a solvent based material printed on top of the multilayer stack. In order to measure the insulating layer thicknesses resulting from the different numbers of subsequent wet-in-wet printing runs, appropriate samples were printed separately on the PET substrate. The thickness was determined using a tactile profilometer DektakXT from Bruker with a pin radius of 2.5 μm and a stylus force of 3 mg.

3. Results

The fully screen printed EL samples were characterized with respect to electrical as well as luminance parameters. Particular attention was paid to the relationship between the characterized values and printing parameters.

3.1 Influence of printing parameters on luminance

For full characterization of the EL panels, an inverter platform was specifically developed in order to control the parameters of the electrical excitation. A maximum output peak-to-peak voltage of up to 400 V_{pp} with any required output waveform could be obtained for frequencies up to 5 kHz (Hirmer, et al., 2016). Compared

to other available inverters (Goncharov, et al., 2017; Assef, et al., 2013), the developed inverter platform can change significantly more parameters and thus characterize the EL panels more extensively.

The luminance, light emission per area in cd/m^2 , was measured with a Gossen MavoMonitor for sinusoidal shaped excitation voltages. As expected, the measurements verified that the luminance is independent of size and shape of the panels. The measurements henceforth were concentrated to one specific layout, a square-shaped panel with an area of 16 cm^2 . It was found that at least two steps for the insulating layer were necessary to safely avoid pinholes and thus short circuits. We observed that printing the insulating layer in only one step yielded to an imprint of the screen, which can be avoided by printing two steps.

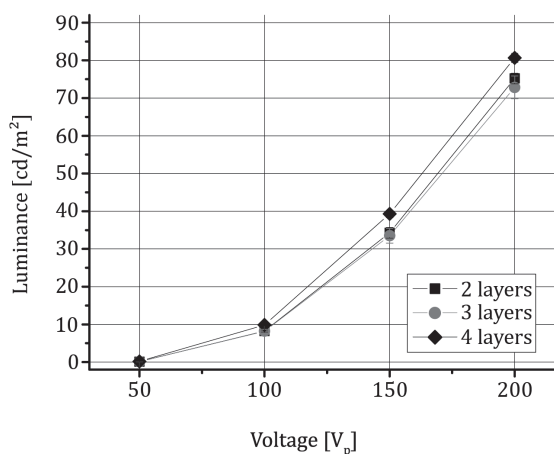


Figure 2: Influence of BaTiO_3 insulating layer thickness on luminance for sinusoidal peak voltage (V_p) waveforms of 5 kHz

We focused on samples with two to four subsequent depositing steps for the insulating layer. As expected, the results of the luminance measurements showed that the luminance was increasing with voltage (see Figure 2).

Table 3: Measured layer thicknesses for the number of printed BaTiO_3 insulating layers

# Printing steps	Layer thickness (average) [μm]
1	25.1 (± 1.4)
2	46.5 (± 4.1)
3	53.1 (± 6.3)

Table 3 shows that the insulating layer thickness is increasing with the number of subsequent printing steps as a function of the number of subsequent wet-in-wet printing. There are two additional observations: Firstly, the ink transfer ratio from the screen

to the substrate, i.e. the increment in layer thickness, became smaller with each repetition. Layer thickness was not a linear function of the number of printing steps. Secondly, the average deviation of the mean layer thickness, i.e. the surface roughness, became gradually larger at the same time. We would have expected that the leveling of the wet printed layer by surface tension was more efficient when layer thickness is large. Apparently, the opposite is true here: leveling of irregularities and smoothing of the surface became worse. We attribute this to a progressing aggregation of the BaTiO₃ particles in the ink, making the material more and more immobile.

Despite the increase of the thickness of the insulating layer with the number of printing steps, the capacitance per area did not increase as expected. In particular, it should be inversely proportional to the thickness values shown in Table 3. Figure 2 shows the influence of two, three and four printed insulating layers on the luminance with sinusoidal excitation peak voltages from 50 V_p to 200 V_p at 5 kHz. One observes a voltage at V₀ ~50 V_p below which there was no light emission.

Above this voltage, luminance increases with $(V - V_0)^2$ where V is the operation voltage. This indicates some nonlinearity in the electro-optical behavior of the panel, specifically at voltages close to V₀. Interestingly, luminance does not significantly change with number of printing steps, and with the dielectric layer thickness. In view of the thickness measurements, one would have expected that capacitance per area and thus luminance decreased. Contrary to this expectation, the maximum of luminance, although being only marginal, was observed with four printed insulating layers (with highest applied voltage of 200 V_p and a frequency of 5 kHz). This interesting phenomenon has important implications on process design and on the structure of equivalent electrical circuits for EL technology. A similar effect has also been reported in an earlier work for pad printed panels (Bodenstein, et al., 2019). Here, this was assigned to an increasing compactification of the porous BaTiO₃ layer with the number of subsequent deposition steps. This aspect will be discussed in Section 4.

3.2 High voltage impedance characterization of electroluminescent panels

Figure 3a shows a complex electrical equivalent circuit model which takes account of the electric features related to the different printed layers (Ono, 1995). The model is intended for the low frequency range. Here, the nonlinear behavior can be observed. The nonlinearities can be assigned to D₁ and D₂ and R_D. This part represents the luminescent layer which can be regarded as a short circuit in lighted condition. For

voltages above V₀ as reported in Section 3.1, a simplified electrical equivalent model as shown in Figure 3b can be used for the inverter design. In lighted condition, the EL panel can be regarded as a serial connection of a resistor R_{PEDOT}, which is related to the transparent front electrode and a parallel connection of C_{EL} and R_{EL}.

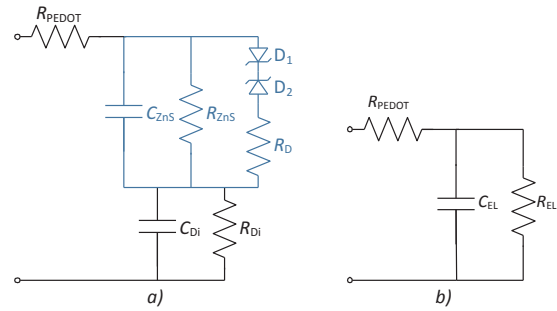


Figure 3: Equivalent circuit of an electroluminescent panel: (a) complex model for off-condition, (b) simplified model for on-condition, since D₁, D₂ and R_D can be neglected in lighted condition; adapted from Ono (1995)

The values for all components of the equivalent circuit can be extracted from impedance measurements. Therefore, all printed panels were characterized with a ModuLab® XM MTS system (AMETEK Scientific Instruments, n.d.). It can measure the impedances of the EL panels with average (root mean square) voltages up to 70 V_{rms} (≈ 200 V_{pp}). Hence, contrary to most characterizations in literature, the panels can be tested above the threshold voltage of the luminescence layer in lightning conditions, i.e. in the nonlinear range. Figure 4 shows exemplarily the Bode plot of a 16 cm² disk EL panel with two layers of insulation in off-condition (1 V_{rms}) and on-condition (70 V_{rms}).

Compared to previous measurements (Ionescu, Drăghici and Bonfert, 2015; Kaiser, Marques and Correa, 2013), the frequency range can be expanded to higher frequencies achieving a better electronic understanding of the panel. Higher frequency characterization is of particular interest if the EL is excited with non-sinusoidal pulse sequences, or if the stray capacitors are of importance, e.g. in capacitive proximity sensors (Hirmer, Saif and Hofmann, 2018).

Figure 4 shows the panel impedance and the phase as a function of operating frequency between 10 Hz and 1 MHz, measured with a low voltage amplitude of 1 V_p (such that the panel is dark), and with 70 V_p (such that the panel is bright). We observe a decrease in impedance for frequencies below ~200 Hz for the bright panel, and an even more substantial phase difference of up to 6° at frequencies below ~10 kHz. Table 4 summarizes these voltage-dependent effects which were extracted at 1 kHz, a typical operation fre-

quency for EL panels. This feature can be assigned to the activation of the bright luminescent layer and is taken in account in the equivalent circuit by the non-linear elements of the ZnS layer.

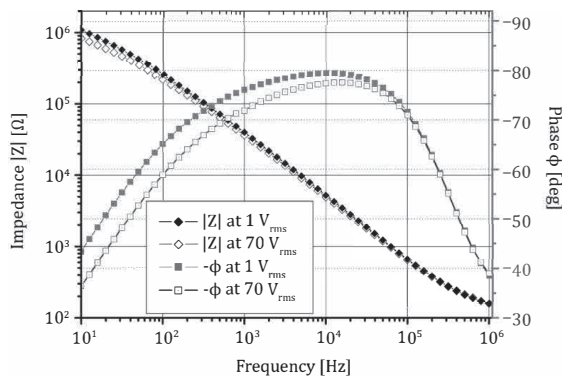


Figure 4: Measured impedance of an EL panel in off ($1 V_{rms}$) and on condition ($70 V_{rms}$)

Table 4: Comparison of the impedance measurement at $1 V_{rms}$ and $70 V_{rms}$ at 1 kHz

Voltage [V_{rms}]	Impedance [Ω]	Phase [$^\circ$]
1	39870.0	-76.1
70	34630.0	-71.9
Ratio	-15.1 %	-5.9 %

The impedance measurement verifies that the impedance of an EL panel cannot be entirely characterized by a capacitor with a serial resistor. A parallel resistor is required as well. It reflects the feature that the phase tends to 0° at $\omega \rightarrow 0$.

3.3 Influence of the $BaTiO_3$ insulating layers on the impedance

As described in Section 2, the EL panels from Batch 1 were printed with up to four different layers of $BaTiO_3$ insulation to investigate the influence of the insulating layer on the overall performance of the panel. As expected, the thickness of the insulating layer is increasing with the number of printed layers (though not in a linear manner, see Table 3).

Following the physics of a parallel plate capacitor, the capacitance is expected to decrease with increasing layers of insulating material. However, measurements in lighted condition ($70 V_{rms}$) revealed a converse behavior as shown in Figure 5. For the sake of comparability, the capacitance was extracted at 100 kHz since the permittivities of the materials are specified by the manufacturer for this frequency. It can be seen that the measured mean capacitance is increasing with the number of insulating layers for all shapes and sizes of the EL panels.

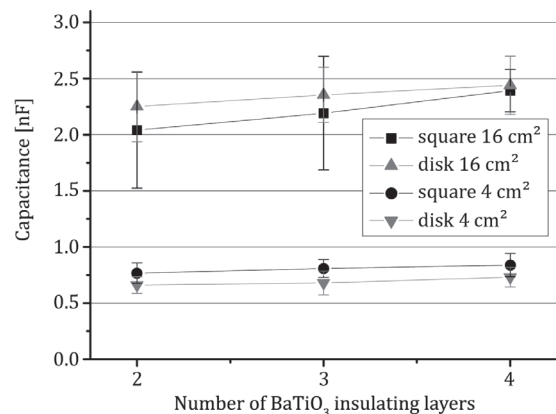


Figure 5: Measured mean capacitance of all printed panels increases with the number of printed $BaTiO_3$ insulating layers

Whereas the thickness is increasing by 14.29 % from two to three layers of insulation, the capacitance is slightly increasing by 7.42 % for 16 cm^2 large square-shaped EL panels. This could be attributed to an increasing compactness of the underlying insulating layer by the additional printing steps. This effect will be discussed in more detail in Section 4.

3.4 Influence of ambient light condition on capacitance measurement

In addition to the influences of printing parameters, we observed that the panel capacitance also depended on the ambient illumination of the panel. Panel capacitance is tentatively smaller under dark than under illuminated condition, but the tendency is not that reproducible in the dark as compared to the illuminated case. With the high voltage impedance measurement equipment, the effect of ambient light can be verified quantitatively. The measured impedances were fitted to the equivalent circuit model shown in Figure 3b with a major focus on C_{EL} and R_{PEDOT} . These two parameters were extracted for on- and off-conditions of the EL at different ambient illumination, i.e. in a dark and a bright environment. The comparison of the extracted capacitance and resistance was referenced to the capacitance value of the high voltage measurement at bright condition $C_{EL}(70 V_{rms,bright})$ since the EL panel is typically used in lighted environments. Hence, this impedance represents the load that the inverter has to drive.

The comparisons of the different operating conditions of the EL measurement setup are shown in Table 5. Compared to the reference $C_{EL}(70 V_{rms,bright})$, the high voltage measurement in the dark does not show significant influences on capacitance. This can be explained by the light emitted by the panel itself (see column 1 in Table 5).

Table 5: Comparison of the measured capacitance at different ambient light conditions and the reference capacitance $C_{EL,ref}$ being $C_{EL}(70 V_{rms,bright})$

	$\frac{C_{EL}(70 V_{rms,dark}) - C_{EL,ref}}{C_{EL,ref}}$	$\frac{C_{EL}(1 V_{rms,bright}) - C_{EL,ref}}{C_{EL,ref}}$	$\frac{C_{EL}(1 V_{rms,dark}) - C_{EL,ref}}{C_{EL,ref}}$
Square 16 cm ² [%]	-6.5	+46.4	-13.9
Disk 16 cm ² [%]	-5.3	+40.8	+4.5
Square 4 cm ² [%]	-6.2	+49.6	-16.5
Disk 4 cm ² [%]	-6.3	+42.0	-2.0

Measuring the capacitance at low voltages shows an excess of capacitance ΔC up to 50 % compared to 70 V_{rms} bright conditions (see column 2 in Table 5). Measurements with low voltages at dark conditions still show a discrepancy of up to -16 % (see column 3 in Table 5). However, this difference is considerably smaller than at bright conditions. Consequently, if only a low voltage capacitance or impedance meter is available, the capacitance of the EL should be characterized in dark conditions (compare Table 5).

For the inverter design, the series resistance R_{PEDOT} is the second important parameter since it determines the maximum current that has to be delivered by the output stage of the inverter. Measurements showed that the resistance can be determined at any voltage, i.e. low or high voltage, and any ambient condition, i.e. dark or bright, leading to a maximum standard deviation of 2.6 %.

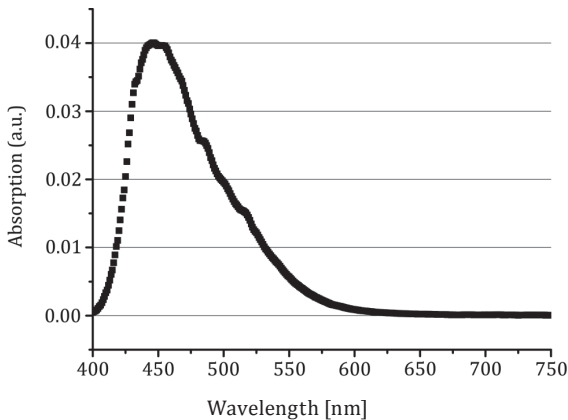


Figure 6: Absorption spectrum of the screen printed electroluminescent panels with a peak at 446 nm

It can be concluded that the operation condition has an enormous influence on the extracted capacitance. We found that ambient light is responsible for this systematic deviation. The absorption spectrum of the screen printed EL panels was measured with a spectrometer, NanoCalc from OceanOptics, Largo, USA. From this it follows that the absorption wavelength peak range center is measured at 446 nm which is in the visible range of light wavelength (see Figure 6).

As molecular absorption and emission of photons are always interconnected, this could explain the origin of the electron-hole-excitation in the luminescent layer which contributes to its polarizability in the electric field. If the EL impedance is measured at voltages which are high enough to excite fluorescence in the ZnS, the absorption of photons from ambient light contributes only few compared to the number of electrically induced electron-hole-pairs. Consequently, ambient light has only little influence on the impedance of the panel. If the device is measured at low voltages, i.e. below the threshold voltage V_0 , no electron-hole-pairs can be created by the electrical field. Therefore, the pairs from absorption of ambient photons provide the majority of mobile charge carriers. Hence, ambient light has significant effect on the electrical parameters at low voltage characterization. For this reason, EL panels should be characterized at dark ambient conditions.

3.5 Influences of luminescent layers on capacitance

As described in Section 2, a second series of EL samples was produced, varying the number of ZnS:Cu:Cl luminescent layers (one to four) with constant number of printing steps of the BaTiO₃ insulating layer (Batch 2). These EL panels enabled investigations of the luminescent layers on the electrical parameters.

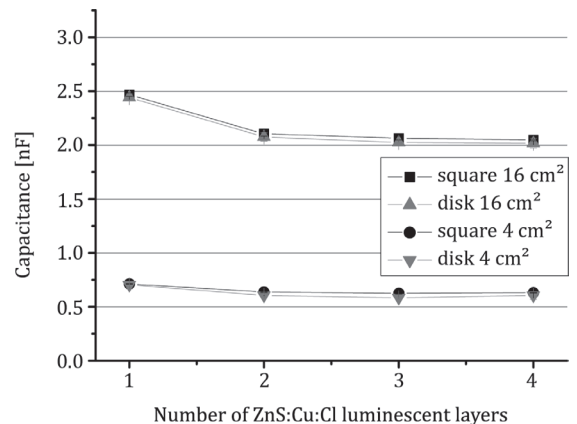


Figure 7: Measured mean capacitance of all printed panels decreases with the number of printed luminescent layers

Figure 7 shows the change of capacitance with increasing number of luminescent layers. It can be seen that the capacitance is slightly decreasing with each deposited layer, in contrast to the tendency found when varying the printing steps of the insulating BaTiO₃ layer where the capacitance is increasing (compare Figure 5). We assign this to the feature that solid ZnS particles have a much lower permittivity than BaTiO₃ particles. The permittivity ϵ_r of ZnS is of order of 6 (Madelung, Rössler and Schulz, 1999), whereas it is of order of 1000 (Adachi, et al., 2001) and more for ferroelectric BaTiO₃ particles. Thus, even if ZnS particles agglomerate in the printed layer as shown in Figure 8, the effect on the total dielectric constant of the layer and thus on capacitance should be much smaller in this case. The increase of layer thickness dominates here the effect of a possible particle compactification within the layer.

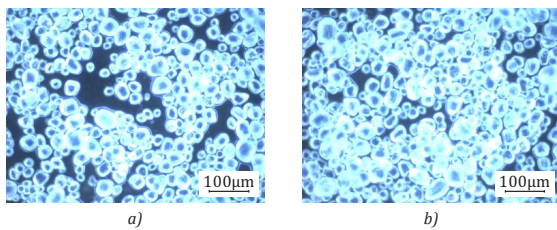


Figure 8: Fluorescent microscopic images of printed layers of ZnS particles for (a) one and (b) two printing steps

Regarding the structure of the EL panel as shown in Figure 1, the capacitance C_{EL} of the EL is composed by two series capacitances. One is determined by the insulating layer and one is determined by the luminescent layer. Hence, the overall capacitance can be calculated by

$$\frac{1}{C_{EL}} = \frac{1}{C_{Insulating}} + \frac{1}{C_{Luminescent}} \quad [1]$$

with the capacitance C_i with i indicating insulating and luminescent, respectively. By using a parallel plate approach, C_i can be calculated using the printing and material data by

$$C_i = \frac{\epsilon_0 \epsilon_{r,i} A}{d_i} \quad [2]$$

with ϵ_0 being the vacuum permittivity, $\epsilon_{r,i}$ being the relative permittivity of the material i , A being the area and d_i being the thickness of the layer. The relative permittivities ϵ_r of the printed composite materials at 100 kHz are given by the manufacturer to 7.5 for the insulation and 3.5 for the luminescent layer, respectively. Using an EL area A of 16 cm², the measured layer thicknesses of Table 3 and a luminescent layer thickness of 51.0 µm, the capacitances can be calculated by Equation [2] and compared to the measured values.

For the square-shaped panel with three printing steps of luminescent layers, it can be seen that the discrepancy of the measured values compared to the calculated series connection C_{EL} is more than 63 % (see penultimate row of Table 6). We tried to extract the reciprocal relative permittivity $1/\epsilon_{r,Luminescent}$ from our data and obtained values close to or even below zero. Regarding the error bars, this may be interpreted as an electrical conductive interlayer with $\epsilon_{r,Luminescent} \rightarrow \infty$. Comparing the calculated capacitances $C_{Insulating}$ to the measurement results in a failure of down to 5.9 %, which proves the statement above (see bottom row of Table 6).

Table 6: Comparison of calculated and measured capacitances for 16 cm² square-shaped panels with three printing steps of the luminescent layer

	min	mean	max
Calculated $C_{Insulating}$ [nF]	1.79	2.00	2.27
Calculated $C_{Luminescent}$ [nF]	0.95	0.97	0.99
Calculated C_{EL} [nF]	0.62	0.65	0.69
Measured $C_{measured}$ [nF]	1.69	2.19	2.70
$\frac{C_{measured} - C_{EL}}{C_{measured}}$ [%]	63.19	70.17	74.40
$\frac{C_{measured} - C_{Insulating}}{C_{measured}}$ [%]	-5.89	8.77	15.81

4. Discussion

The electrical impedance of printed EL panels depends on and hence can be designed by the manufacturing process of the different layers of the panel stack. The front electrode, i.e. its limited electrical sheet conductivity, has a foreseeable and well understood impact and can be accounted for by a series resistor R_{PEDOT} in our electrical low-frequency impedance model. Manufacturing details of the insulating and the luminescent layers show quite unexpected effects. Even more surprising was the significance of nonlinear electrical panel behavior in our experiments. Its impedance depends significantly on the operation voltage and even on the light exposure of the panel.

It was shown that the capacitance of the panel is a function of the number of subsequently printed insulating layers. We did not always observe a decrease in capacitance and light emission when the layer thicknesses were increased. For the insulating BaTiO₃ layer, we could indeed verify that multiple wet-in-wet overprinting increased the final layer thickness. However, no decrease in panel capacitance was found. We assign this to a progressing compactification of the BaTiO₃ particles in the layer. Even if this compactification was

small from the point of view of layer morphology, the dielectric effect could be significant because the specific dielectric polarizability of barium titanate is extremely large compared to the binder polymer. Even a small reduction of porosity of the particle network dispersed in the UV curable polymer varnish should yield a large increase in the overall ϵ_r of the compound. For the printing process, this implies that wet-in-wet application of additional material will not only increase the layer thickness but may also affect the morphology of the particulate network in the already deposited fraction of the layer. This may, in case of high ϵ_r -powders such as BaTiO₃, result in an increased polarizability, compensating the effect of the increasing layer thickness. Using dispersions of only small or average polarizability such as ZnS, this latter effect may be unrecognized. This interpretation also explains the increase of light emission that was observed in panels made with multiple insulating layer printing steps (see Figure 2).

Considering the luminescent ZnS layer, another effect appears. Although panel capacitance decreased with the thickness of the ZnS layer as qualitatively expected, the capacitor exhibited voltage- and radiation-related sensitivities. Our experiments clearly imply that this must be related to the ZnS not to the BaTiO₃ layer. Increasing operation voltage from 1 V_{rms} to 70 V_{rms} in a frequency range between 10 Hz and ~10 kHz revealed an additional dielectric loss. The phase $\Phi(\omega)$ significantly decreased from the low voltage value by ~6°. The point here is not that the phase is higher than -90° as one would expect for a capacitor with loss-free dielectrics, but rather that the observed loss angle found at low operation voltage increased when switching to high voltages. One also finds some effect in the absolute impedance $|Z(\omega)|$, but this is small and may easily escape under the measurement noise.

We represented the nonlinearity in our equivalent electrical circuit model by two inversely oriented Zener diodes D₁ and D₂ as shown in Figure 3a. In addition, two resistors R_D and R_{ZnS} are provided to describe the impedance of the device. The Zener diodes represent the threshold voltage V₀ associated with the onset of light emission of the EL panel. This is explained in Figure 2.

Physically this means, that the contribution of the luminescent layer to dielectric polarizability disappears as soon as light emission is active. The ZnS apparently behaves more like a conductor than like a polarizable insulator and it virtually appears to be no longer present in the capacitor. In this state, the BaTiO₃ layer seems to be the only dielectric layer as calculations in Table 6 show. This behavior could be explained by the electron-hole pairs which are excited across the band gap of ZnS in the electric field. These electron-hole pairs are responsible for light emission

by their recombination. Charge carrier recombination takes some time which is of order of few nanoseconds, typically. In this period, however, they contribute to current transport. The excited ZnS exhibits a small but finite conductivity (Kobayashi, et al., 1973; Kaiser, Marques and Correa, 2013), comparable to the conductivity of e.g. ionic electrolytes.

According to the Drude model of electron-related conduction in solids, this corresponds to a dielectric constant with a frequency-dependent imaginary part, i.e.

$$\epsilon_r(\omega) \sim 1 + i \frac{\omega_p^2 \tau}{\omega} \quad [3]$$

where ω_p is the excitation frequency of the electron-hole pair and τ is the characteristic life time of the excited state. The Drude model allows to calculate the phase difference $\Delta\Phi(\omega)$ between the non-excited state (where the free charge carrier related fraction of the imaginary part of ϵ_r vanishes) and the excited state. This is given by

$$\tan \Delta\phi(\omega) \sim \frac{\omega_p^2 \tau}{\omega} \quad [4]$$

and implies that the phase difference should scale as 1/ ω and disappear with increasing frequency. This was qualitatively confirmed by the measurements (see Figure 4). For these reasons, thickness and layer porosity of the luminescent layer drop out of the specific capacitance in the on-state of the panel. They are still of some relevance in the off-state.

Electron-hole pairs can also be created in zinc sulfide by optical absorption. This feature is an evident characteristic of luminescent ZnS in contrast to nonluminescent materials like BaTiO₃ as was used in the insulating layer. It explains the observed nonlinear dependence of electrical impedance, namely of the parallel resistances on the illumination of the panel.

5. Conclusions

This work focuses on the nonlinear behavior of fully screen printed electroluminescent panels. For the first time, investigations showed the influences of high voltage characterization in comparison to low voltage characterization. From the impedance measurements it can be concluded that the impedance of an electroluminescent panel changes depending on operation voltage and illumination due to the activation of the ZnS:Cu:Cl luminescent layer. This effect is most pronounced at lowest frequencies when one compares impedance measurements taken at low and at high voltages. In doing so, the ambient light is absorbed within the luminescent layer. Furthermore, the high voltage impedance measurement showed that the

thickness of luminescent layer and its morphology is almost insignificant for the overall capacitance of the panel in contrast to the features of the insulating layer.

The measurements imply that an increase in insulating layer thickness leads to a decrease of porosity of that layer which in turn increases the capacitance of the fully screen printed electroluminescent panels. For the first time, the high voltage measurement of

complex impedance showed the differences of on- and off-condition of the electrical parameters of electroluminescent panels. Our experiment indicates that electroluminescent panels, when adequately driven with alternating voltages, could also be interesting alternatives for printed optical or radiation sensors, since photon absorption and pair creation in the ZnS layer can immediately be detected in a characteristic change of the electrical properties.

Acknowledgement

The authors would like to acknowledge the support by Franz Binder GmbH & Co. to make their luminance measurement system available and Henkel Electronic Materials for providing silver ink used in this work.

References

- Adachi, C., Tokito, S., Tsutsui, T. and Saito, S., 1988. Electroluminescence in organic films with three-layer structure. *Japanese Journal of Applied Physics*, 27(2A), pp. L269–L271. <https://doi.org/10.1143/JJAP.27.L269>.
- Adachi, M., Akishige, Y., Asahi, T., Deguchi, K., Gesi, K., Hasebe, K., Hikita, T., Ikeda, T., Iwata, Y., Komukae, M., Mitsui, T., Nakamura, E., Nakatani, N., Okuyama, M., Osaka, T., Sakai, A., Sawaguchi, E., Shiozaki, Y., Takenaka, T., Toyoda, K., Tsukamoto, T. and Yagi T., 2001. BaTiO₃ (hexagonal) [F] Survey, 1A-10. In: Y. Shiozaki, E. Nakamura and T. Mitsui, eds. *Ferroelectrics and related substances: oxides*. Berlin, Heidelberg: Springer Verlag. <https://doi.org/10.1007/b53034>.
- AMETEK Scientific Instruments, n.d. *ModuLab XM MTS – Materials Test System*. [online] Available at: <<http://www.ameteki.com/products/materials-testing-systems/modulab-xm-mts>> [Accessed 06 March 2019].
- Assef, A.A., Maia, J.M., Schneider, F.K., Button, V.L.S.N. and Costa, E.T., 2013. A reconfigurable arbitrary waveform generator using PWM modulation for ultrasound research. *Biomedical Engineering OnLine*, 12: 24. <https://doi.org/10.1186/1475-925X-12-24>.
- Bodenstein, C., Sauer, H.M., Dörsam, E. and Hirmer, K., 2018. Influence of printing parameters in fully pad-printed electroluminescence panels on curved surfaces. In: *19th International Society of Coating Science and Technology Symposium (ISCST)*. Long Beach, CA, USA, 16–19 September 2018.
- Bodenstein, C., Sauer, H.M., Hirmer, K. and Dörsam, E., 2019. Printing process and characterization of fully pad printed electroluminescent panels on curved surfaces. *Journal of Coatings Technology and Research (online first)*.
- Goncharov, I.N., Kabyshev, A.M., Kozyrev, E.N. and Maldzigaty, A.I., 2017. Power source for electroluminescent panels. *Journal of Communications Technology and Electronics*, 62(6), pp. 634–637. <https://doi.org/10.1134/S1064226917060080>.
- Hirmer, K., Saif, M.B. and Hofmann, K., 2018. Integrated symmetrical high voltage inverter for the excitation of touch sensitive electroluminescent devices. In: *2018 IEEE 30th International Symposium on Power Semiconductor Devices and ICs (ISPSD 2018)*. Chicago, IL, USA, 13–17 May 2018. Piscataway, NJ, USA: IEEE, pp. 343–346.
- Hirmer, K., Schuster, P., Keil, F. and Hofmann, K., 2016. Low-cost high-voltage arbitrary waveform generator for broad lifetime measurements of electroluminescent devices. In: *2016 2nd Annual Southern Power Electronics Conference (SPEC 2016)*. Auckland, New Zealand, 5–9 December 2016. Piscataway, NJ, USA: IEEE, pp. 155–158.
- Ionescu, C., Drăghici, F. and Bonfert, D., 2015. A SPICE model for electroluminescent foils. In: *2015 38th International Spring Seminar on Electronics Technology (ISSE 2015)*. Eger, Hungary, 6–10 May 2015. Piscataway, NJ, USA: IEEE, pp. 526–531.
- Kaiser, W., Marques, R.P. and Correa, A.F., 2013. Light emission of electroluminescent lamps under different operating conditions. *IEEE Transactions on Industry Applications*, 49(5), pp. 2361–2369. <https://doi.org/10.1109/TIA.2013.2260315>.
- Kim, J.-Y., Bae, M.J., Park, S.H., Jeong, T., Song, S., Lee, J., Han, I., Yoo, J.B., Yung, D. and Yu, S., 2011. Electroluminescence enhancement of the phosphor dispersed in a polymer matrix using the tandem structure. *Organic Electronics*, 12(3), pp. 529–533. <https://doi.org/10.1016/j.orgel.2010.12.020>.
- Kobayashi, H., Tanaka, S., Sasakura, H. and Hamakawa, Y., 1973. The electron injection mechanism of the electroluminescent ZnS: Tb³⁺ films. *Japanese Journal of Applied Physics*, 12(12): 1854. <https://doi.org/10.1143/JJAP.12.1854>.
- Lee, T.-M., Hur, S., Kim, J.-H. and Choi, H.-C., 2010. EL device pad-printed on a curved surface. *Journal of Micromechanics and Microengineering*, 20(1): 015016. <https://doi.org/10.1088/0960-1317/20/1/015016>.

- Madelung, O., Rössler, U. and Schulz, M. eds., 1999. Zinc sulfide (ZnS) dielectric constant, cubic modification. In: *Landolt-Börnstein – Group III Condensed Matter 41B (II-VI and I-VII Compounds; Semimagnetic Compounds)*. Berlin, Heidelberg: Springer Verlag. https://doi.org/10.1007/10681719_392.
- Ono, Y.A., 1995. *Electroluminescent displays*. Singapore: World Scientific Publishing. <https://doi.org/10.1142/2504>.
- Ranfeld, C., 2010. *Drucktechnische Herstellung eines funktionalen Demonstrators*. Diplomarbeit. Technische Universität Chemnitz.
- Ranfeld, C., Theopold, A. and Dörsam, E., 2011. Flexographic printing for the production of inorganic electroluminescent devices. In: *Proceedings of Printing Future Days 2011: 4th International Scientific Conference on Print and Media Technology*. Chemnitz, Germany, 7–10 November 2011. Berlin: VWB Verlag.
- Sauer, H.M., Ranfeld, C. and Dörsam, E., 2010. An investigation of the screen printing process for electroluminescent panels and the influence of printing parameters on the performance of the panels. In: *Electronics Convention proceedings, LOPE-C 2010 scientific paper: LOPE-C, Large-Area, Organic & Printed Electronics Convention: International Conference and Exhibition for the Organic and Printed Electronics Industry*. Frankfurt, Germany, 31 May–2 June 2010. Frankfurt, Germany: OE-A.

JPMTR 126 | 1907
 DOI 10.14622/JPMTR-1907
 UDC 655.1|62.7:005.2

Research paper
 Received: 2019-07-10
 Accepted: 2019-09-05

An approach to risk-based maintenance strategy of a printing press

Avijit Kar and Arun Kiran Pal

Department of Printing Engineering, Jadavpur University,
 Salt Lake Campus, Block-LB, Plot-8, Sector-III, Salt Lake
 Kolkata-700098, India

karavijit29jet@gmail.com
 arunkiranpal@gmail.com

Abstract

The unexpected failures, downtime associated with breakdown and make ready, loss of production and higher maintenance costs are the major problem in any printing press. Risk based maintenance strategy helps in designing an alternative methodology to minimise the risk by identifying the breakdown pattern and then increasing the reliability. Reliability analysis is necessary for every type of machinery for fault detection, risk assessment and evaluation, and maintenance planning. The probability of failures that hinder the reliability can be influenced by some technical, administrative or management actions. The aim of the proposed study is to analyse reliability and availability for maintenance planning on the basis of risk index and overall equipment effectiveness. And maintenance of equipment is prioritized based on the risk which helps in reducing the overall risk of the press.

Keywords: reliability, availability, risk index, overall equipment effectiveness

1. Introduction

Plant's machine and equipment will not remain safe or reliable if it is not maintained properly. General objective of the maintenance process of a machine is to achieve the possible safety with the lowest possible cost. In the present study the concept of risk-based maintenance (RBM) strategy has been adopted to identify the high risk machines and then attempts have been made to minimize the actual failure rate with a statistical approach. This helps us to minimize any unexpected production loss due to various components' downtime. The present study is conducted on the basis of regular visits to the printing press continuously for three months in order to get appropriate data. These data are processed and then analysed so that tolerable risk can be achieved.

2. Theoretical background of the study

2.1 Maintenance strategy

The basic aim of maintenance strategy is to minimize hazards which are caused by the unexpected failure of the equipment. To increase the machine's life and to reduce the risks caused by failure of the equipment, risk-based approaches are used in present days.

Risk-based approach is a technique for identifying, characterizing, quantifying, and evaluating the loss from an event. Risk analysis approach integrates probability and consequence analysis at various stages (Khan and Haddara, 2013). Risk assessment can be quantitative or qualitative. The output of a quantitative risk assessment will typically be a number. The number (i.e. cost impact per unit time) could be used to prioritize a series of risked items. Risk can be written as given in Equation [1].

$$\text{Actual risk} = \text{Failure probability} \times \text{Consequence of failure} \quad [1]$$

The proposed RBM strategy aims at reducing the overall risk of failure of the operating facilities. In areas of high and medium risk, a focused maintenance effort is required. The RBM suggests a set of recommendations on how many preventive tasks are to be performed. The implementation of RBM will reduce the likelihood of an unexpected failure. The RBM methodology is comprised of following three main modules which are interactively linked. These are risk determination (which consists of risk identification and estimation), risk evaluation (in where acceptance criteria are set to compare with existing risk) and maintenance planning (in where reduction of risk level is executed by the help of proper planning).

2.2 Failure analysis

Failure is an event that affects not only a system but the system criteria also. On a given system the failures may change with the change of time. Failures do not generally occur at a uniform rate, but follow a specific distribution with time as shown in Figure 1. This distribution can be divided into three regions (Dhillon, 2008), namely infant mortality period (where the failure rate progressively improves), useful life period (where the failure rate remains constant) and wear-out period (where failure rates begin to increase).

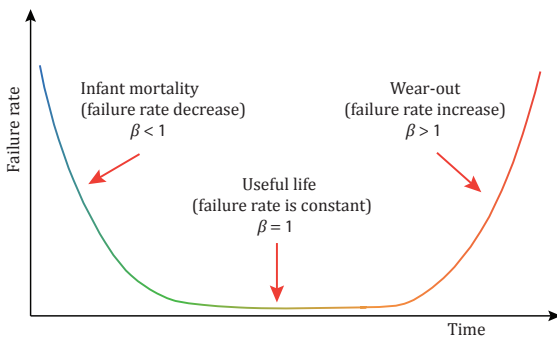


Figure 1: Bath-tub curve of a system describing failure rates at different periods

To the best of the knowledge Weibull distribution is the most widely used distribution in reliability engineering and the failures caused by fatigue, corrosion, mechanical abrasion, diffusion and other degradation processes can be easily analysed. The two parameter Weibull distribution needs two factors, namely scale factor (η) and shape factor (β). Beta (β) describes the shape of the distribution. If $\beta > 1$, the failure rate is increasing due to the accelerated wear and tear of components. If $\beta < 1$, the failure rate is decreasing due to early stage of machine. When the failure rate is constant (for $\beta = 1$), the distribution follows exponential probability law and when failure rate is not constant (i.e. non-linear hazard model) it follows Weibull distribution.

It is also important to note that failure probability is also termed as unreliability in failure analysis. Moreover, if the type of distribution is not known in advance, then the distribution that best fits the failure or repair times can be found using different statistical methods. Anderson-Darling (AD) test (Anderson and Darling, 1952) is used to find best-fit or goodness-of-fit tests which can be implemented with great ease by the use of software tools or Weibull analysis. The AD test is the popular test that determines whether the given set of data is drawn from the probability distribution. In addition to its use as a test of fit for distributions, it can be used in parameter estimation as the basis of minimum distance estimation procedures. It will also help to take decision for choosing the most appropri-

ate statistical distribution method. It is known that lowest AD test value posses best fitted distribution, for example among the three probability distribution like normal, exponential and Weibull, AD value is the lowest for Weibull distribution for its best distribution pattern (Murthy, Xie and Jiang, 2004).

2.3 Reliability analysis

Reliability can also be described as the probability that an item or process operates properly for a specified amount of time under stated conditions (both environmental and operational conditions) without failure (Kumar, 2016). The cumulative density function for reliability $R(t)$ is denoted as $F(t)$ which is also related to failure probability and in combination with the fact that the area under the probability density function (PDF) (denoted as $f(t)$) is always equal to 1. Obviously, the reliability function $R(t)$ can be expressed by Equation [2].

$$R(t) = 1 - F(t) = 1 - \int_0^t f(t)dt \tag{2}$$

The mathematical formulations of PDF for normal, exponential and Weibull distribution plotting are given in Equations [3], [4] and [5].

$$f(t) = \frac{1}{\sigma} \cdot \sqrt{2\pi} \cdot e^{-\frac{(t-\xi)^2}{2\sigma^2}} \tag{3}$$

$$f(t) = \lambda e^{-\lambda(t-\gamma)} \tag{4}$$

$$f(t) = \left(\frac{\beta}{\eta}\right) \cdot \left(\frac{t}{\eta}\right)^{\beta-1} \cdot e^{-\left(\frac{t}{\eta}\right)^\beta} \tag{5}$$

where ξ is mean of time between failure (MTBF), σ is standard deviation of MTBF, λ is the scale parameter, γ is the location parameter, η is characteristic life or scale parameter, β is shape factor value and t is operating time.

Moreover, the technique of AD test and linear regression analysis confirms the validity of use of Weibull distribution for the different components of the printing press. The analysis determines the best-fit line in the least square sense. The least square test has been used to obtain the rate of failure. Linear regression analysis has been carried out by using the probability Equation [6] (Bose, et al., 2013).

$$R_{x,f(x)} = \frac{p}{q} \tag{6}$$

where

$$p = \Sigma[x \cdot f(x)] - \frac{[\Sigma x \cdot \Sigma f(x)]}{N}$$

$$q = \sqrt{\left[\Sigma(x^2) - \frac{(\Sigma x)^2}{N}\right] \cdot \left\{\Sigma f(x^2) - \frac{[\Sigma f(x)]^2}{N}\right\}}$$

x is breakdown time, $f(x)$ is cumulative percentage of failure, N is total operating time, $R_{x/f(x)}$ is correlation coefficient. From the concept of probability, it is known that the correlation coefficient must be in between +1.0 to -1.0. If the correlation coefficient estimates positive value, then the failure rate is increasing and so Weibull distribution can be applied for the estimation of reliability (Kar, 2019).

2.4 Availability analysis

Availability is the probability that a system is not failed or undergoing a repair action/maintenance job when it needs to be used. So the estimation of availability plays vital role for both reliability and maintainability aspects. Availability or inherent availability A_{in} is the function of preventive or scheduled maintenance action and it is expressed (Leitch, 1995) by Equation [7].

$$A_{in} = MTBF / (MTBF + MTTR) \quad [7]$$

where MTTR is defined as the mean time to repair. In real operation administration delay time and logistic delay time should be taken into consideration. Operational availability A_{op} is the probability that a system or equipment, when used under stated conditions in an actual operational environment, will operate satisfactorily. It may be expressed by Equation [8].

$$A_{op} = MTBF / (MTBF + MDT) \quad [8]$$

where MDT is the mean downtime that includes restoration delay time, logistics delay time and administrative delay time.

2.5 Estimation of consequence and risk index

This study also deals with the estimation of consequence and risk index which are very much essential for maintenance planning. The important expressions for consequences and risk index (Khan and Haddara, 2003) are given in Equations [9] and [10].

$$\text{Consequence} = MC + PLC \quad [9]$$

where MC represents machine cost and PLC represents production loss cost of the respective components.

$$\text{Risk index} = \text{Actual risk} / \text{Acceptable risk} \quad [10]$$

2.6 Overall equipment effectiveness

The effectiveness of facilities is its best possible return generated and calculated as percentage of each group of six big losses (Maideen, et al., 2016). The six big losses are breakdown, set-up and adjustments, small stops, reduced speed, production rejects or scraps and

start-up losses. The identified losses can be measured in terms of overall equipment effectiveness (OEE) which is a function of availability, performance rate and quality rate as expressed by Equation [11].

$$\text{OEE} = \text{Availability (\%)} \times \text{Performance rate (\%)} \times \text{Quality rate (\%)} \quad [11]$$

where

$$\text{Availability} = \left(\frac{\text{Planned prod. time} - \text{Unplanned downtime}}{\text{Planned prod. time}} \right) \cdot 100 \%$$

$$\text{Performance} = \left(\frac{\text{Actual prod. output}}{\text{Expected prod. output}} \right) \cdot 100 \%$$

$$\text{Quality} = \left(\frac{\text{Actual prod. input}}{\text{Actual prod. output}} \right) \cdot 100 \%$$

Planned production time is nothing but the loading time for the job (Kar, 2019) in which total observation time is taken where planned downtime is not considered, i.e.

$$\text{Planned prod. time} = \text{Observation time} - \text{Planned downtime} \quad [12]$$

Planned downtime is the machine setup time, loading and unloading time, schedule maintenance time or schedule breaks, etc.

On the other hand unplanned downtime is simply the minor stoppage time loss, sudden breakdown time loss, idle time, uncertain changeover time loss for loading and unloading of material, machine breakdown and its corresponding setup time loss, etc., which are directly concerned with the losses related to availability and performance. It is also important to mention that production output is the combination of production input and rework item and scrap.

3. Press and its components

The present study is conducted in the production system of a daily newspaper company situated in Kolkata, India. One of the key processes of this production system is the web fed offset printing process which has one number of four colour web-offset printing machine. The print production house has the following components shown in Table 1. It is also important to mention that press has two compressors but only one compressor has been taken into consideration for the study as the second compressor is used for emergency backup purpose only.

Table 1: Different components (machines) used in the print production house (approximate values)

Component	Manufacturer	Year of manufacture	Plate size (mm)	Printing area (mm)	Capacity
Web-offset four colour press (printing machine)	Orient Xcell	2009	780 × 510	700 × 395	41200 impressions/h
Computer to plate 1 (CTP 1)	Epson	2014	780 × 510	–	20 plates/h
Computer to plate 2 (CTP 2)	Epson	2009	780 × 510	700 × 395	15 plates/h
Exposure unit	Technova	2005	780 × 510	–	30 plates/h
Compressor	–	2009	–	–	–

4. Data collection and analysis

Basic data collected from the printing press are operating time, breakdown time and number of failures of the components. Data collected for web-offset printing machine is given in Appendix A. Time between failures of different machines has been compiled from the daily maintenance reports during the period from 1st August to 31st October 2018. During this investigation the average temperature inside the press was 28–32 °C and average relative air humidity was 70–80 %. Moreover, as the printing job was mostly associated with newsprint thus the press uses the paper of the same grammage and printing was done mainly in night shift though 35 % of the printing was done in both day and night shifts. Furthermore, it is assumed that the operational conditions are the same for all the machines.

It has been observed that the correlation coefficients of the different components of the press show positive values. Hence Weibull distribution is applied in the present study.

Failure probability for different components has been estimated by Equation [6] and the reliability function for the components has been calculated by using Equation [2]. Table 2 shows the corresponding results of the failure and reliability analysis for different components of the press.

Table 2: Reliability and failure probability of different components

Component	Failure probability	Reliability (%)
Printing machine	0.553	44.69
CTP 1	0.735	26.46
CTP 2	0.539	46.10
Exposure unit	0.777	22.33
Compressor	0.178	82.22

Figure 2 shows Weibull plot for regression analysis of web-offset printing machine. It also shows the values of shape and scale parameters, i.e. $\beta = 1.840$ and $\eta = 283.73$, which were estimated by Minitab17.

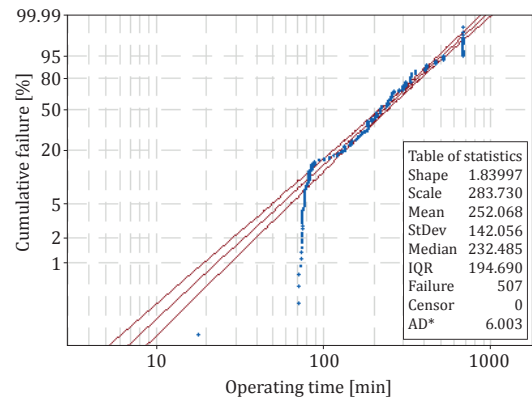


Figure 2: Weibull plot of web-offset printing machine obtained from Minitab17

Figure 3 shows the distribution of PDF that describes the failure characteristics of the printing machine by using software Minitab17.

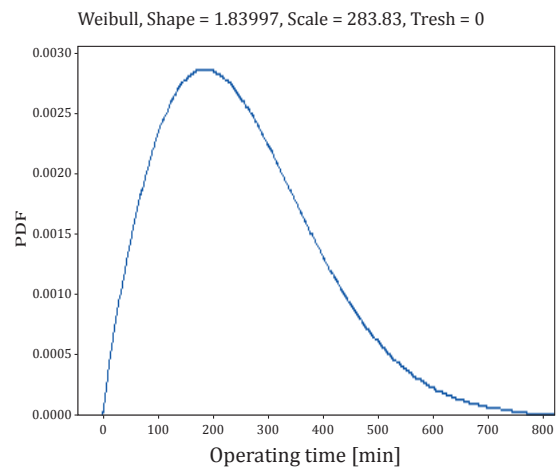


Figure 3: PDF distribution of printing machine obtained from Minitab17

Figure 4 shows the probability plots of the printing machine obtained by normal, exponential and Weibull distribution. It is clear from Figure 4 that Weibull analysis is appropriate as it is best fitted and its AD value is lowest (i.e. 6.003) from the normal and exponential analysis.

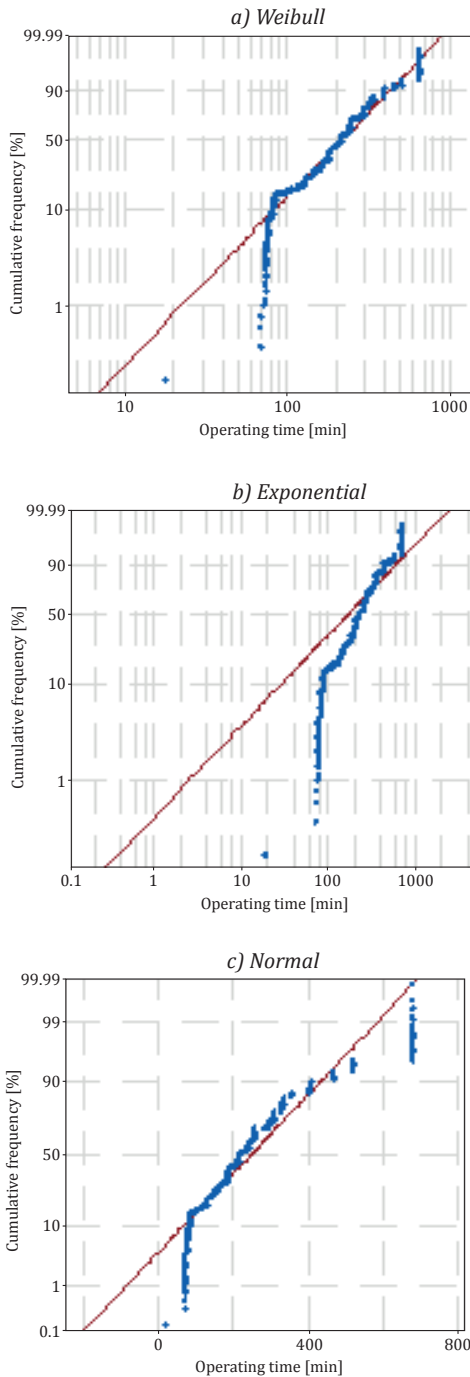


Figure 4: Probability plot of printing machine deriving Anderson-Darling value obtained from Minitab17 (Anderson-Darling (adj): (a) Weibull = 6.003, (b) Exponential = 49.444, (c) Normal = 14.219)

The estimation of availability for web-offset printing machine is described in Appendix B. Figure 5 shows the corresponding availability plot.

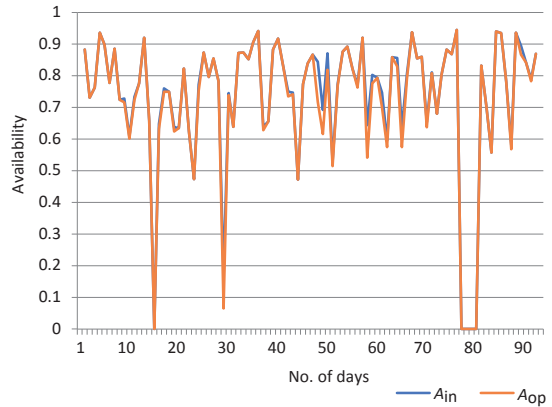


Figure 5: Availability of web-offset printing machine in the period of 92 days

The availability of different components of the press are shown in Figure 6 which indicates that both type of availability of the exposure unit possess low availability. This may be due to the loading and unloading which have been considered as failure. Whereas printing machine and compressor possess high availability during three months under study.

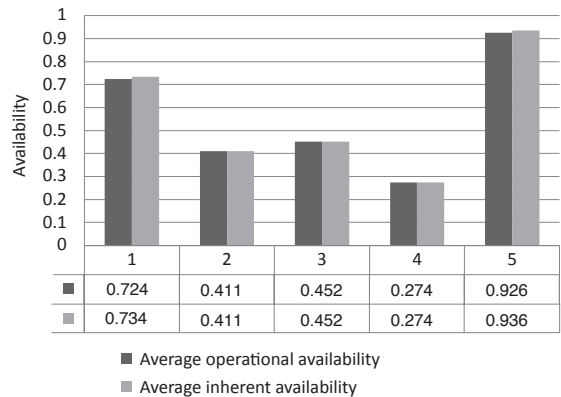


Figure 6: Bar diagram of various availability of components: 1 – printing machine, 2 – CTP 1, 3 – CTP 2, 4 – exposure unit, 5 – compressor

Considering acceptable risk criteria of 2252.05 EUR which is obtained from accounts department of the press, risk indices of different components are shown in Table 3. It is seen that exposure unit is having highest failure rate but after risk analysis it is clear that the web-offset printing machine of the press is facing the maximum failure and risk scenario. This may be due to the high consequences of the printing machines.

Moreover, make-ready time and change-over adjustment time for the printing machine are higher than that of the other components.

Table 3: Consequence, failure probability, actual risk (calculated from Equation 1) and risk index of different components

Component	Consequence (EUR)	Failure probability	Actual risk (EUR)	Risk index
Printing machine	10 062.29	0.553	5 565.79	2.47
CTP 1	543.96	0.735	400.05	0.18
CTP 2	294.72	0.539	158.85	0.07
Exposure unit	319.58	0.777	248.23	0.11
Compressor	460.53	0.178	81.88	0.04

On the basis of risk level, Pareto analysis of all the components of the printing press has been done by using Minitab17, results are shown in Figure 7. Which equipment is needed to be chosen for maintenance planning can be decided from this Pareto analysis.

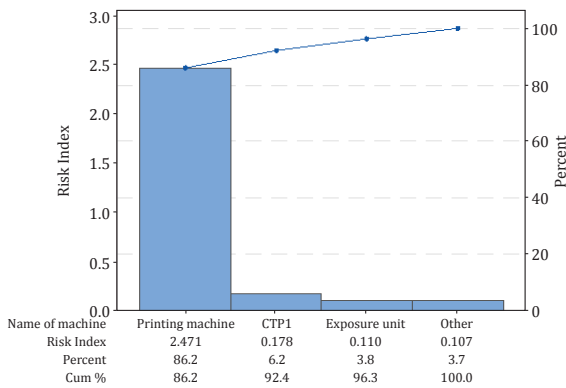


Figure 7: Overall Pareto analysis of different components

The OEE of the component is measured on the basis of high risk. Here web-offset printing machine is at high risk thus OEE of web-offset printing machine is calculated here (Table 4).

Table 4: The overall equipment effectiveness of the printing machine

Parameter	Value
Observation time (min)	20 472
Planned production time (min)	19 436
Planned downtime (min)	1 036
Unplanned downtime (min)	4 539
Operating time (min)	14 886
Actual production output	7 737 591
Capacity per given time (impressions/min)	687
Expected output (impressions)	10 226 682
Amount defect and reproduced (impressions)	96 364
Availability loss (%)	76.65
Performance loss (%)	75.66
Quality loss (%)	98.75
OEE (%)	57.27

From these calculated losses, the OEE for four colour web-offset printing machine is determined from Equation [11] and found to be 57.27 %. Therefore, it is clear that OEE confirms the validity of high risk components. It indicates that this component requires further maintenance planning for improvement.

5. Maintenance planning

The strategy for maintenance planning should be adopted to lower the risk to meet the acceptable criterion, to reduce the probability of failure, to reduce the failure number and AD value, and thus to increase the reliability, availability and OEE.

Table 5: Risk reduction results for the printing machine

Parameter	Value
Actual risk (EUR)	5 565.79
Target (modified) probability of failure	0.224
Risk reduction (EUR)	2 252.05
Modified reliability	0.776

Table 5 shows that the risk (in EUR) had decreased to 2 252.05 EUR (which is the safe limit of acceptable risk criteria) from 5 565.79 EUR and its corresponding probability of failure also decreased from 0.553 to 0.224. Therefore the modified probability of failure for web-offset four colour printing machine is 0.224. As a result reliability will also increase from 44.69 % to 77.62 %. Now the suitable preventive maintenance time interval (i.e. time interval for repair, servicing or replacement) can be estimated from corresponding reliability functions. And this is the approach towards risk-based maintenance to improve overall efficiency of a printing press.

6. Conclusion

The reliability prediction of the printing press depends on the failure frequency and availability pattern of each component. Here the maintenance program has been presented based on the reduction of the risk factor.

This approach ensures that reliability of components is increased after implementation of maintenance planning suggested. This will contribute to the availability of the plant as well as its safe operation.

The present study also helps to identify the critical components based on risk factor and overall equipment effectiveness factor. It can be concluded that by adapting risk-based maintenance analysis or technique it can be easily analysed as to when and which machine is to be checked and replaced by the help of Pareto analysis. Also this technique can be used to find a suitable preventive maintenance interval. The study

undoubtedly confirms that the risk-based maintenance strategy works precisely well in a printing press.

After determining the probability of failure as function of a controllable factor (interval period between preventive maintenance), management has a mechanism to adjust the risk for the studied process. The proposed methodology influences not only risk management but also knowledge management because it is a quantitative method to estimate probabilities of failures and associated costs. Finally, this quantitative methodology may support top management in complying with the requirements of quality management standard.

References

- Anderson, T.W. and Darling, D.A., 1952. Asymptotic theory of certain “goodness of fit” criteria based on stochastic processes. *The Annals of Mathematical Statistics*, 23(2), pp. 193–212. <http://dx.doi.org/10.1214/aoms/1177729437>.
- Bose, D., Ghosh, G., Mandal, K., Sau, S.P. and Kumar, S., 2013. Measurement and evaluation of reliability, availability and maintainability of a diesel locomotive engine. *International Journal of Scientific and Research Publications*, 3(9).
- Dhillon, B.S., 2008. *Mining equipment reliability, maintainability, and safety*. London: Springer Verlag.
- Kar, A., 2019. *Evaluation of reliability, availability and maintainability of a printing press*. Master Thesis. Jadavpur University.
- Khan, F. and Haddara, M., 2003. Risk-based maintenance (RBM): a quantitative approach for maintenance/inspection scheduling and planning. *Journal of Loss Prevention in the Process Industries*, 16(6), pp. 561–573. <https://www.doi.org/10.1016/j.jlp.2003.08.011>.
- Kumar, P., 2016. *Reliability, availability and maintainability analysis of the main conveyor system in underground coal mine: a case study of Churha (RO) mine*. Master Thesis. National Institute of Technology Rourkela.
- Leitch, R.D., 1995. *Reliability analysis for engineers: an introduction*. Oxford, New York: Oxford University Press.
- Maideen, N.C., Sahudin, S., Mohd Yahya, N.H. and Norliawati, A.O., 2016. Practical framework: implementing OEE method in manufacturing process environment. *IOP Conference Series: Material Science and Engineering*, 114(1): 012093. <https://www.doi.org/10.1088/1757-899X/114/1/012093>.
- Murthy, D.N.P., Xie, M. and Jiang, R., 2004. *Weibull Models*. Hoboken, New Jersey: John Wiley & Sons.

Appendix A: Data of web-offset printing machine for failure analysis

The collected basic data for the printing machine in press section is as follows. Cumulative failure y has been calculated by using the Equation [A1].

$$y_{i+1} = \frac{F_{i+1}}{\sum_{i=0}^n F_i} + F_i \quad [A1]$$

For calculation of correlation coefficient $R_{x,f(x)}$ the Equation [6] was used.

Day No.	Operating time (min)	Breakdown time (min)	No. of failures	Cumulative failure (%)
1	75	10	2	0.39
2	209	81	9	2.17
3	356	111	8	3.75
4	131	9	2	4.14
5	71	8	3	4.73
6	77	22	3	5.33
7	77	10	2	5.72
8	76	29	2	6.11
9	331	131	11	8.28
10	302	200	11	10.45
11	157	60	5	11.44
12	83	24	2	11.83
13	115	10	2	12.23
14	75	39	5	13.22
15	0	0	0	13.22
16	186	108	16	16.37
17	300	100	9	18.15
18	147	49	4	18.93
19	88	53	5	19.92
20	85	49	4	20.71
21	102	22	4	21.50
22	78	47	3	22.09
23	194	216	12	24.46
24	204	67	6	25.64
25	124	18	3	26.23
26	86	22	2	26.63
27	77	13	2	27.02
28	83	23	4	27.81
29	18	257	1	28.01
30	258	91	11	30.18
31	246	139	10	32.15
32	164	24	3	32.74
33	83	12	2	33.14
34	75	13	2	33.53
35	77	8	1	33.73
36	80	5	1	33.93
37	186	110	8	35.50
38	248	130	7	36.88
39	150	20	4	37.67
40	78	7	1	37.87
41	108	22	4	38.66
42	75	27	4	39.45
43	186	65	6	40.63

Day No.	Operating time (min)	Breakdown time (min)	No. of failures	Cumulative failure (%)
44	175	196	7	42.01
45	239	70	9	43.79
46	161	31	5	44.77
47	78	12	2	45.17
48	286	113	6	46.35
49	223	139	9	48.13
50	203	45	3	48.72
51	310	293	25	53.65
52	411	124	14	56.41
53	240	34	6	57.59
54	83	10	2	57.99
55	74	16	2	58.38
56	255	79	9	60.16
57	81	7	1	60.36
58	257	218	14	63.12
59	204	59	5	64.10
60	127	33	2	64.50
61	147	63	5	65.48
62	134	99	13	68.05
63	474	78	12	70.41
64	682	140	25	75.35
65	219	162	24	80.08
66	528	140	12	82.45
67	75	5	1	82.64
68	253	43	6	83.83
69	331	54	8	85.40
70	340	194	17	88.76
71	408	97	9	90.53
72	168	79	5	91.52
73	262	64	5	92.50
74	83	11	2	92.90
75	79	12	2	93.29
76	86	5	1	93.49
77	0	0	0	93.49
78	0	0	0	93.49
79	0	0	0	93.49
80	0	0	0	93.49
81	144	29	3	94.08
82	171	72	6	95.27
83	82	65	3	95.86
84	95	6	1	96.06
85	86	6	2	96.45
86	183	51	6	97.63
87	122	93	4	98.42
88	89	6	1	98.62
89	85	13	2	99.01
90	80	15	2	99.41
91	79	22	2	99.80
92	73	11	1	100.00

 $N = 14886$ $\sum x = 5575$ $\sum F = 507$ $\sum f(x) = 4728.99$ $p = 269883$ $q = 487917$ $R_{x/f(x)} = 0.55$

Appendix B: Estimation of availability of printing machine

The estimation of availability for web-offset printing machine is as follows (for abbrevs and quantities refer to text).

Day No.	Operational time (min)	Failure no.	MTBF (min)	Down time (min)	Repair time (min)	MTTR (min)	A_{in}	MDT (min)	A_{op}
1	75	2	37.5	10.0	10.0	5.0	0.882	5.0	0.882
2	220	9	24.5	81.0	81.0	9.0	0.731	9.0	0.730
3	356	8	44.5	111.0	111.0	13.9	0.762	13.9	0.762
4	131	2	65.5	9.0	9.0	4.5	0.936	4.5	0.935
5	71	3	23.7	8.0	8.0	2.7	0.899	2.7	0.898
6	77	3	25.7	22.0	22.0	7.3	0.778	7.3	0.777
7	77	2	38.5	10.0	10.0	5.0	0.885	5.0	0.885
8	76	2	38.0	29.0	29.0	14.5	0.724	14.5	0.723
9	331	11	30.1	131.0	124.0	11.3	0.727	11.9	0.716
10	302	11	27.5	200.0	195.0	17.7	0.608	18.2	0.601
11	157	5	31.4	60.0	57.0	11.4	0.734	12.0	0.723
12	83	2	41.5	24.0	24.0	12.0	0.776	12.0	0.775
13	115	2	57.5	10.0	10.0	5.0	0.920	5.0	0.920
14	75	5	15.0	39.0	39.0	7.8	0.658	7.8	0.657
15	0	0	0.0	0.0	0.0	0.0	0.000	0.0	0.000
16	186	16	11.6	108.0	101.0	6.3	0.648	6.8	0.630
17	300	9	33.3	100.0	95.0	10.6	0.759	11.1	0.750
18	147	4	36.8	49.0	49.0	12.3	0.750	12.3	0.750
19	88	5	17.6	53.0	50.0	10.0	0.638	10.6	0.624
20	85	4	21.3	49.0	49.0	12.3	0.634	12.3	0.634
21	102	4	25.5	22.0	22.0	5.5	0.823	5.5	0.822
22	78	3	26.0	47.0	47.0	15.7	0.624	15.7	0.624
23	194	12	16.2	216	216.0	18.0	0.473	18.0	0.473
24	204	6	34.0	67.0	60.0	10.0	0.773	11.2	0.752
25	124	3	41.3	18.0	18.0	6.0	0.873	6.0	0.873
26	86	2	43.0	22.0	22.0	11.0	0.796	11.0	0.796
27	77	2	38.5	13.0	13.0	6.5	0.856	6.5	0.855
28	83	4	20.8	23.0	23.0	5.8	0.783	5.8	0.783
29	18	1	18.0	257.0	90.0	90.0	0.167	257.0	0.065
30	258	11	23.5	91.0	88.0	8.0	0.745	8.3	0.730
31	246	10	24.6	139.0	139.0	13.9	0.638	13.9	0.638
32	164	3	54.7	24.0	24.0	8.0	0.872	8.0	0.872
33	83	2	41.5	12.0	12.0	6.0	0.874	6.0	0.873
34	75	2	37.5	13.0	13.0	6.5	0.852	6.5	0.852
35	77	1	77.0	8.0	8.0	8.0	0.906	8.0	0.905
36	80	1	80.0	5.0	5.0	5.0	0.941	5.0	0.941
37	186	8	23.3	110.0	105.0	13.1	0.639	13.8	0.628
38	248	7	35.4	130.0	130.0	18.6	0.656	18.6	0.656
39	150	4	37.5	20.0	20.0	5.0	0.882	5.0	0.882
40	78	1	78.0	7.0	7.0	7.0	0.918	7.0	0.917
41	108	4	27.0	22.0	22.0	5.5	0.830	5.5	0.830
42	75	4	18.8	27.0	25.0	6.3	0.750	6.8	0.735
43	186	6	31.0	65.0	63.0	10.5	0.746	10.8	0.741
44	175	7	25.0	196.0	196.0	28.0	0.472	28.0	0.471
45	239	9	26.6	70.0	70.0	7.8	0.773	7.8	0.773
46	161	5	32.2	31.0	31.0	6.2	0.839	6.2	0.838
47	78	2	39.0	12.0	12.0	6.0	0.867	6.0	0.866
48	286	6	47.7	113.0	53.0	8.8	0.844	18.8	0.716
49	223	9	24.8	139.0	99.0	11.0	0.693	15.4	0.616
50	203	3	67.7	45.0	30.0	10.0	0.871	15.0	0.818
51	310	25	12.4	293.0	276.0	11.0	0.529	11.7	0.514

Day No.	Operational time (min)	Failure no.	MTBF (min)	Down time (min)	Repair time (min)	MTTR (min)	A_{in}	MDT (min)	A_{op}
52	411	14	29.4	124.0	120.0	8.6	0.774	8.9	0.768
53	240	6	40.0	34.0	34.0	5.7	0.876	5.7	0.875
54	83	2	41.5	10.0	10.0	5.0	0.892	5.0	0.892
55	74	2	37.0	16.0	16.0	8.0	0.822	8.0	0.822
56	255	9	28.3	79.0	76.0	8.4	0.770	8.8	0.763
57	81	1	81.0	7.0	7.0	7.0	0.920	7.0	0.920
58	257	14	18.4	218.0	142.0	10.1	0.644	15.6	0.541
59	204	5	40.8	59.0	50.0	10.0	0.803	11.8	0.775
60	127	2	63.5	33.0	33.0	16.5	0.793	16.5	0.793
61	147	5	29.4	63.0	50.0	10.0	0.746	12.6	0.700
62	134	13	10.3	99.0	91.0	7.0	0.595	7.6	0.575
63	474	12	39.5	78.0	78.0	6.5	0.859	6.5	0.858
64	682	25	27.3	140.0	115.0	4.6	0.856	5.6	0.829
65	219	24	9.1	162.0	126.0	5.3	0.635	6.8	0.574
66	528	12	44.0	140.0	128.0	10.7	0.805	11.7	0.790
67	75	1	75.0	5.0	5.0	5.0	0.938	5.0	0.937
68	253	6	42.2	43.0	43.0	7.2	0.855	7.2	0.854
69	331	8	41.4	54.0	54.0	6.8	0.860	6.8	0.859
70	340	17	20.0	194.0	180.0	10.6	0.654	11.4	0.636
71	408	9	45.3	97.0	95.0	10.6	0.811	10.8	0.807
72	168	5	33.6	79.0	79.0	15.8	0.680	15.8	0.680
73	262	5	52.4	64.0	64.0	12.8	0.804	12.8	0.803
74	83	2	41.5	11.0	11.0	5.5	0.883	5.5	0.882
75	79	2	39.5	12.0	12.0	6.0	0.868	6.0	0.868
76	86	1	86.0	5.0	5.0	5.0	0.945	5.0	0.945
77	0	0	0.0	0.0	0.0	0.0	0.000	0.0	0.000
78	0	0	0.0	0.0	0.0	0.0	0.000	0.0	0.000
79	0	0	0.0	0.0	0.0	0.0	0.000	0.0	0.000
80	0	0	0.0	0.0	0.0	0.0	0.000	0.0	0.000
81	144	3	48.0	29.0	29.0	9.7	0.832	9.7	0.832
82	171	6	28.5	72.0	72.0	12.0	0.704	12.0	0.703
83	82	3	27.3	65.0	65.0	21.7	0.558	21.7	0.557
84	95	1	95.0	6.0	6.0	6.0	0.940	6.0	0.940
85	86	2	43.0	6.0	6.0	3.0	0.935	3.0	0.934
86	183	6	30.5	51.0	51.0	8.5	0.782	8.5	0.782
87	122	4	30.5	93.0	88.0	22.0	0.580	23.3	0.567
88	89	1	89.0	6.0	6.0	6.0	0.937	6.0	0.936
89	85	2	42.5	13.0	10.0	5.0	0.895	6.5	0.867
90	80	2	40.0	15.0	15.0	7.5	0.842	7.5	0.842
91	79	2	39.5	22.0	21.0	10.5	0.790	11.0	0.782
92	73	1	73.0	11.0	11.0	11.0	0.869	11.0	0.869



JPMTR 127 | 1820
DOI 10.14622/JPMTR-1820
UDC 676.2:547.4/667.6

Research paper
Received: 2018-12-06
Accepted: 2019-09-05

The starch addition to a curtain coating formulation and its effect on pitting

Samantha L. Schoenfelder, Alexandra Pekarovicova and Paul D. Fleming

Center for Printing and Coating Research,
Western Michigan University,
4601 Campus Drive, A-217 Floyd Hall, Kalamazoo, MI 49008

a.pekarovicova@wmich.edu

Abstract

An undisclosed recycled fiber board mill installed a “two-slotted” curtain coater to replace an air knife coater, which enabled a high-quality coating without past speed limitations. With the curtain coater’s installation, however, a prominent defect arose, known as “pitting”. Pitting occurs when the coating of the sheet has small holes that mar its surface, which, when clustered together or larger in size, can cause print break-up. Starch was added to the formulation to modify rheological properties of top and bottom curtain coatings, and advance water retention capabilities of them. Results show the original formulations with no starch were more thixotropic than the starch formulations. Starch aided in reducing the low shear viscosity by as much as 25 %, which had a large impact on converting the system from a strongly elastic rheology to a more viscous one. Such a move toward a more purely viscous system helped to prevent the elastic stretching and reduced bubble formation in the coatings. Starch addition also increased water retention capabilities of the coatings. The pitting significantly decreased during these trials, with lower overall pit counts and area pitted.

Keywords: coating color, coated paperboard, air entrapment, rheology, surface free energy

1. Introduction and background

The utilization of recycled paperboard within the packaging industry creates a competitive need to continuously improve production by finding advancements to create a superior product in a timely and cost-effective manner. These engineering advancements assist in manipulating production, while maintaining quality and trialing new applications to promote the highest optimization for the paper machine. Changes can be made at all parts of the process, from source of fiber over the coating, to actual machinery installations as new modifications are developed. It is an ever changing, developing industry, which does not have the option for complacency.

Curtain coating is currently a more and more chosen method for single or multiple coating layer applications for high speed coating of various coat weights, ensuring smaller pores than obtained with other coating methods, leading to better print quality (Birkert, et al., 2006). Curtain liquid coating is falling freely, with gravity accelerating the falling curtain, until it falls

on the moving substrate (Becerra and Carvalho, 2011; Liu, et al., 2016). Certain operating parameters need to be held in the “coating window”, otherwise various defects may occur. High speed of web compared to curtain velocity causes bead pulling forward, but on the other hand, slow web movement compared to curtain velocity causes its upstream movement, so called heel formation. Air entrainment underneath of liquid bead may be caused by too high web speeds and lastly, the curtain may break into columns at its very low flow rate (Becerra and Carvalho, 2011).

A single curtain coating layer employs a curtain slot die as well as a curtain slide die. For multiple film applications, curtain slide dies are mostly used. Curtain coating is becoming popular in cardboard grades for packaging (Döll, 2010). One of the drawbacks of the process is the air entrainment, creating bubbles in the coating. Air entrainment has been cited as the leading cause of pitting (Figure 1) in theoretical and experimental capacities, occurring between substrate and impinging coating, because of interfacial tension constraints (Urscheler, et al., 2005).



Figure 1: SEM image of pitted surface of curtain coated board

The air film is unstable and breaks into bubbles, creating visible defects (pits/craters) that are usually related to the curtain's coating interface in contact with the base coat that is in contact with the substrate (Urscheler, et al., 2005). Most curtain coaters have a vacuum device installed near the impingement zone, which acts as a deaerator, but these do not always have the capacity to remove all the boundary air that can cause entrainment and lead to pitting. Therefore, as web speeds increase, the removal of boundary layer air becomes progressively more difficult by the vacuum and manifests itself as the onset of air-entrapment in the impingement zone (Tripathi, 2005; Tripathi, et al., 2009). For very high web speeds, steam substitution (Tripathi, 2005; Tripathi, et al., 2009), where saturated steam is injected before the impingement zone to remove boundary layer air, may be applied. Furthermore, roughness of a substrate and poor wettability may lead to a higher amount of air entrainment. Without a direct metering device, the substrate does not require special strength properties for good runnability (Renvall, et. al., 2013), but a curtain will follow the contour of low/high amplitude roughness. With a high frequency of varying roughness, the coating film becomes more complex and sometimes incapable of keeping its form, where high base sheet roughness may create craters (Figure 2) (Tripathi, 2005).

Both figures (Figure 1 and Figure 2) show visible pits on the top coated layer. Air entrainment is also synonymous with dynamic wetting failure, with critical parameters being speed and viscosity (Becerra and Carvalho, 2011; Liu, et al., 2016), but also found to be dependent on surface tension (Marston, et al., 2009). In order to fully understand wetting, one must look at viscosity and surface tension as tools to combat the effects of high speeds and lower the possibility of air entrapment. In the case of high speed curtain coater equipped with saturated steam, the environment is

defined by the temperature of steam used to eliminate air at the interface. This raised temperature of the coating leads to a rapid and significant drop in viscosity of the coating, especially a decrease in the viscoelasticity. However, the dual slotted curtain coater discussed here does not facilitate steam substitution, since it is totally enclosed, although has temperature and air relative humidity control (21–24 °C, 50 % RH). Thus, other solutions must be sought to control pitting.

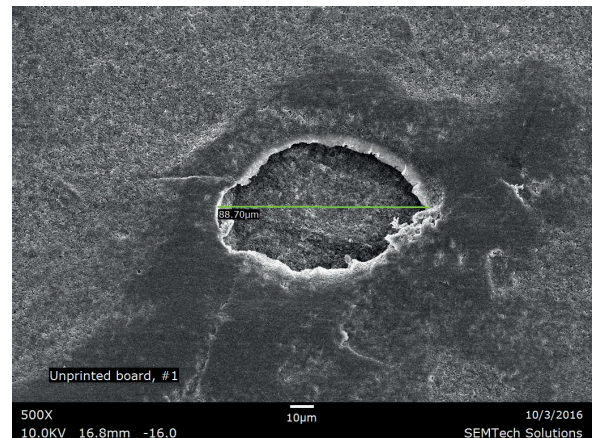


Figure 2: SEM image of large pit on curtain coated board

Curtain coating suspensions are known to be pseudo-plastic, which means that they are shear-thinning, or their viscosities decrease as the shear rate increases. It has been suggested that rheological properties of the coating are critical to avoid or reduce the presence of pitting, because they influence how easily air bubbles can be extracted from the coating color (Tripathi, 2005; Triantafillopoulos, et al., 2004; Kistler, 1983).

Thus, in order to deter air entrainment, the promotion of wetting through rheological properties is critical at impingement as it affects the process in multiple ways. As the liquid coating displaces gas at a dynamic wetting line (when the coating meets the web), it will create a continuous film of coating that is deposited on the moving substrate (Kistler, 1983). Close to the respective wetting lines, there are comparatively short regions of rapidly rearranging shear and extensional flow, which is even more complicated with non-Newtonian fluid-like coating (Kistler, 1983). Low coating viscosity can cause a splash to occur at the web, while extensional viscosity is the key to preventing heel forming (Tripathi, 2005; Chen, et al., 2016), both highly affecting the amount of air that will be dragged under the film. Thus, rheological properties of the coating are critical to avoid or reduce the presence of pitting, because they influence how easily air bubbles can be extracted from the coating color (Tripathi, 2005). As previously stated, the air entrainment will then form bubbles, which lead

to pitting. Curtain stability cannot only be improved with a thicker curtain, greater curtain velocity, and higher volumetric flow rate per unit width, but also with a lower coating surface tension (Brown, 1961).

Thus, surface tension is an important component of a coating, particularly at slow speed. It was also found through experimentation that the air entrainment phenomenon is strongly dependent on surface tension, a fact already well established for various other coating methods (Marston, et al., 2009; Klass, 2004). Lowering surface tension can result in higher viscous drag on the curtain, increasing the radius of curvature of the pulled film over the impingement zone, and reducing total pressure, resulting in delayed and reduced air entrainment (Tripathi, et al., 2009). Without proper wettability, air entrainment is promoted between the coating and the substrate, and the coating will literally not adhere to the substrate (Chen, 1992; Pekarovicova and Fleming III, 2005; BASF, 2016). The aim of this work was to focus on a coating (and board) related defect known as, “pitting” or “pinholes,” which causes an abnormal surface of the board that will not print smoothly. This issue was occurring at a recycled board plant, which has been troubleshooting it since their air knife coater was replaced by a curtain coater. In this work, coating formulations were altered to fight pitting.

2. Materials and methods

2.1 Procedures

Experiments were done on a Fourdrinier paper machine, using 100 % recycled fiber material to produce a three-ply paperboard, running at 460–610 m/min (1500–2000 fpm). The three plies consisted of a top liner, filler, and back liner, with caliper of 0.457 mm (18 mills or 18 pt). The board was first bar precoated, and then submitted to high speed two slotted curtain coating, done wet-on-wet at ambient temperature. The original curtain coater formulations for the top and base curtain coatings are found in the Table 1.

Table 1: The DF base and top coatings original basic formulation (pph – parts per hundred parts of pigment)

Materials	DF base original basic formulation (pph)	DF top original basic formulation (pph)
Clay	100.00	90.00
TiO ₂	0.00	10.00
Latex	21.00	21.00
Thickener	0.35	0.35
Dispersant	0.12	0.12
Surfactant	0.30	0.30

The addition of 3 parts of a dry starch product per hundred parts of pigment (pph) to the base and top direct fountain (DF) coatings was made to see the effects on pitting (Table 2). The trial samples rheology, Brookfield viscosity, high-shear viscosity, and water retention value (WRV) were tested and compared to the control (original formula) formulation’s measurements. Starch origin, molecular weight and its properties were proprietary, and thus they cannot be revealed. However, it was expected that starch exhibits a typical proportion of amylose and amylopectin.

Table 2: Formulation of DF base and top coating for trial with added starch (pph – parts per hundred parts of pigment)

Materials	DF base starch trial (pph)	DF top starch trial (pph)
Clay	100.00	90.00
TiO ₂	0.00	10.00
Latex	21.00	21.00
Thickener	0.25	0.25
Dispersant	0.12	0.12
Surfactant	0.30	0.30
Starch	3.00	3.00

The modified DF base coating formulation (Table 2) first had 0.35 pph of thickener and 2 pph of starch, which increased Brookfield viscosity from ~400 mPa·s to ~600–700 mPa·s at a shear rate of 26.3 s⁻¹ and it was seen as an operational concern to the mill. It is above target for the suggested Brookfield viscosity, and it started to cause physical build-up in the system. To ensure long-term success, it was decided to lower the thickener from 0.35 pph to 0.25 pph, and increase the starch from 2 pph to 3 pph. This brought the viscosity down to ~300–350 mPa·s.

Viscosity (in mPa·s) of the coatings was measured by a Brookfield DV-E viscometer at 100 RPM with the (RV) spindle #3 at a shear rate of 26.3 s⁻¹ at 25 °C. The high shear viscosity was measured on a Hercules DV-10 viscometer with an E-Bob. The averages of three measurements of a ramp up from 0 s⁻¹ to 46288 s⁻¹ shear rate (0–4 400 RPM) back down to 0 s⁻¹ (0 RPM) per coating at 25 °C were recorded.

The WRV determinations were done on coated samples that were taken from the paper machine and tested by the AA-GWR Water Retention Meter (model 250) by Kaltec Scientific, Inc. according to TAPPI Standard T-701 pm-01 (TAPPI, 2005). Solids content was measured using an IR heated balance until constant sample weight was achieved. Instrument software calculated solids content automatically. Density of the wet coating was determined gravimetrically using weight per gallon stainless steel cups.

2.2 Pitting tests

A pitted sample was stained with a Croda manufactured red drawdown ink (MBR 10039) to better see the pitting on the sheet. This also makes it easier for the image analysis software to read. There are three numbers that help determine the amount of pitting on the sheet: large pit count, proportion of pitted area (in %), and overall number of pits per measured area, which was 6 mm × 6 mm.

Each trial assessment requires a paper tester to look at four random and separate areas of the sheet in the cross-machine (CD) direction. The large pit count is taken with a Barska brand handheld digital microscope (AY11336), with a 10–300 × magnification, which is placed on the stained sheet. The higher magnification, but lower resolution highlights larger pits, and dulls out the smaller pits, showing only large pits are in the visual area of interest (greater than 1 mm in diameter). The paper tester rates the sample on a scale of 1–4. Thus, after four tests, the lowest pit count is ranked 4 and the highest is 16. According to claims filed against the mill, printing issues tend to occur when the large pit count reaches ranking of about an 8. There is obviously variability in data due to the dependency on human perception and opinion. The proportion of pitted area and number of pits were both found through the use of a 200 × magnification Aven brand digital microscopic camera (Mighty Scope NIR 5M). A public domain software, ImageJ, was used to analyze these images, which is able to distinguish pits through the contrast of color (pits are darker red, filled in by the Croda ink). It digitally computes the average proportion of pitted area and number of pits through the four measurements.

3. Results and discussion

Through SEM images (Figures 3 and 4), it's easy to see the differences in depth and width of the pits and caves, which range from smaller pinhole-like sizes, to larger crater-like that are 80 μm wide or larger, both of which can be up to over 20 μm deep. Figure 3 clearly shows a pit crater on the top coating layer, whereas in Figure 4 can be seen caves in one or the other DF coated layers or possibly in between the two. Through experimentation and research, causes of pitting have been narrowed down to a few mechanisms: air entrapment, wetting of the substrate (governed by physical and chemical behaviors such as coating properties), and substrate roughness (Lee, et al., 2009). All three are interconnected, and can be addressed by certain coating properties. Moisture within the sheet was also suspected, but through multiple trials deemed a less critical mechanism at this point; varying drying tem-

peratures were tried twice and found inconclusive, and without a statistical effect on pitting. Challenges faced within the paperboard industry have been the need to develop the right formulations to operate at higher flow rates, higher solids, higher curtain heights, and high web speeds compared to the photographic and specialty paper applications (Tripathi, 2005). Thus, in order to successfully know how to combat pitting, it is useful to understand what exacerbates the defect, and how the coating formulation can be manipulated to reduce it.

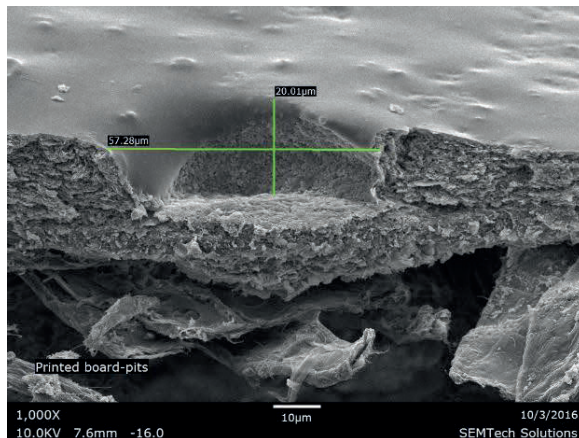


Figure 3: SEM cross-section image of a pit

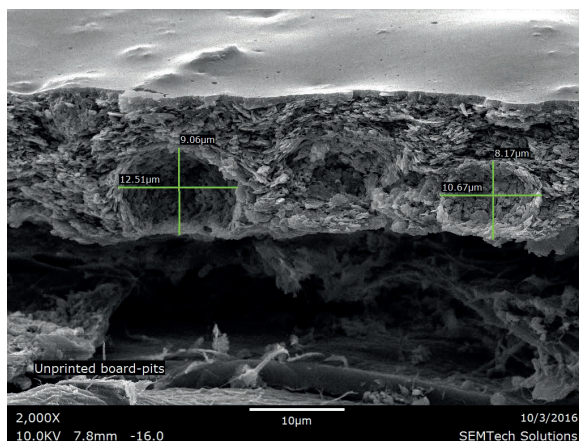


Figure 4: SEM image of cross-section cave pitting / air entrapment under the surface

The original DF top and base coating formulations can be seen in Table 1. A brief analysis of the board was performed in order to better understand the surface on which the coating is applied (Table 3). It is known that pitting only occurs when the rod precoat and the curtain coatings are all applied and does not occur when only the precoat or the curtain coatings are applied. Thus, a comparison of the coated paperboard and the precoated paperboard was completed to see any similarities and/or differences that might reveal any indications behind the pitting phenomena.

Table 3: Uncoated vs. precoated paperboard – summary of paper properties, average (AVG) and standard deviations (STD), from Schoenfelder (2017)

Test	Uncoated paperboard	Precoated paperboard
Surface free energy (mJ/m ²)	70.7	46.6
Dispersive component (mJ/m ²)	31.1	43.9
Polar component (mJ/m ²)	39.6	3.7
Porosity – Gurley (s/100 cm ³)	AVG 48.0	850.0
	STD 6.0	107.0
Roughness – PPS (μm)	AVG 6.6	4.5
	STD 0.4	0.3
Roughness – Sheffield Units (SU)	AVG 304.0	260.0
	STD 8.0	26.0

Three major properties of the board were of interest: surface free energy, smoothness/roughness, and porosity. Surface free energy (mJ/m²) of the board will help to quantify the interactions between the surface and the liquid coating (surface tension), and therefore provides an insight into the wetting of the paperboard at the dynamic wetting line. Smoothness or roughness is of importance since it was noted in the Introduction that a rougher sheet could allow for more boundary air entrainment. Porosity (more correctly permeability) is of interest, since a greater porosity will allow for more wetting, where the coating will tend to dive into the sheet; this could also allow air and moisture to escape through more passages, where a less porous sheet will force air and moisture through the top of the coating. The averages of ten individual readings of all properties (besides surface free energy, which was calculated using various contact angle measurements and the Owens and Wendt (1969) method), were calculated and are summarized in Table 3. The surface free energy of the uncoated board is considerably higher than the precoated board (Table 3), which will result in faster, more complete wetting of a liquid on the surface. This value is probably skewed, due to the high porosity of the sheet, which will contribute to the wetting of the surface and produce a false surface free energy value; a Cobb test confirmed this theory, as there was complete wetting in less than 1–2 seconds on the uncoated surface.

The DF top and base coating formulations were modified by adding 2 pph of dry starch to an ~3.6 t (8000 lb.) batch of each coating (Table 4). Otherwise, the coating formulations stayed the same. Static surface tension of both coatings was measured. For starch coating, its value was slightly higher than that of original (control) one (Figure 5).

The DF base starch formulation would run first, in order to ensure curtain stability and machine runnability. If the run was smooth, the operators would then

transition the starch into the DF top slot as well. It was planned to run on 0.457 mm (18 pt) board, but due to the unpredictability of machine runs and customer demands, the trial was run on 0.356 mm (14 pt) board.

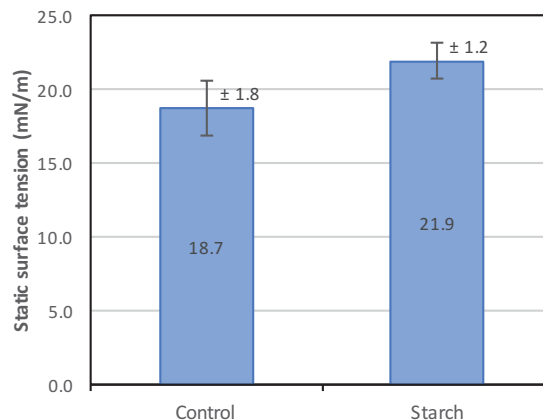


Figure 5: Static surface tension (SFT) for control coating vs. starch coating

Later, also other calipers were tested. Long-term results (Schoenfelder, 2017) of pitting on different caliper boards are given in Table 4. The average proportion of pitted area showed a significant decrease from 4.1 % to 2.6 % (Table 5), with each caliper showing a substantial drop in area, besides 0.558 mm (22 pt), which stayed virtually the same. There is also less variability in pitting, with lower standard deviations, which means there is more predictability in the product outcome through the use of starch.

Coating samples were taken at the DF curtain head, and WRV were monitored to better indicate when the starch was fully integrated into the system (the WRV value was expected to decrease with the addition of starch).

Pit counts immediately dropped from 8 to 5 when the DF base trial coating reached the DF head; proportion of pitted area decreased from 5.8 % to 3.6 %. This decrease in pitting was consistent within the duration of the trial, with the overall large pit counts decreasing to an average of 4.1 % and pitted area decreasing to 2.6 % after both DF base and top trial coating batches reached the DF head. Pre-trial pitting is illustrated at the Figure 6 and the decrease in pitting after starch addition is shown in Figure 7.

The coating rheology could be manipulated by the addition of starch to promote further healing properties and increase water retention capabilities.

It is possible that the amylose starch linear structures with no side chains in the starch mixture are responsible for such behavior, where it's also known to be

Table 4: Longterm average (AVG) and standard deviations (STD) data of caliper vs. pitting for starch added in DF base (Schoenfelder, 2017)

Grade / Caliper	Large pit count		Proportion of pitted area (%)		Number of pits	
	AVG	STD	AVG	STD	AVG	STD
0.356 mm (14 pt)	4	1	3.1	1.2	4958	1941
0.406 mm (16 pt)	5	1	2.8	1.2	4608	2062
0.457 mm (18 pt)	4	0	2.6	1.2	4434	1915
0.508 mm (20 pt)	4	0	2.4	1.0	4236	2131
0.533 mm (21 pt)	4	0	2.6	0.7	4730	1395
0.558 mm (22 pt)	4	0	3.7	1.3	6487	2255
Overall AVG	4	1	2.6	1.1	4521	2033

Table 5: Starch trial summary – pitting averages (AVG) and standard deviations (STD) viewed from an area of 6 mm × 6 mm

	Large pit count		Proportion of pitted area (%)		Number of pits	
	AVG	STD	AVG	STD	AVG	STD
Control / pre-trial	7	1	4.1	0.9	5300	1100
Trial – starch	4	1	2.6	0.8	2900	310

hydrophilic in nature. Vinyl acrylic latex may have side chains or copolymers in their chain, with unknown amounts of -COOH groups, and side branches of various amounts and sizes, all of which may affect packing of polymer molecules in the coating and thus affect viscosity. The original formulation (control) and the

starch trial formulation (with the decreased thickener component) were both tested for the following basic coating properties: surface tension (Figure 5), density (Figure 8), solids content (Figure 9), Brookfield viscosity (Figure 10), high shear viscosity vs. shear rate (Figure 11), and water retention values (Figure 12).

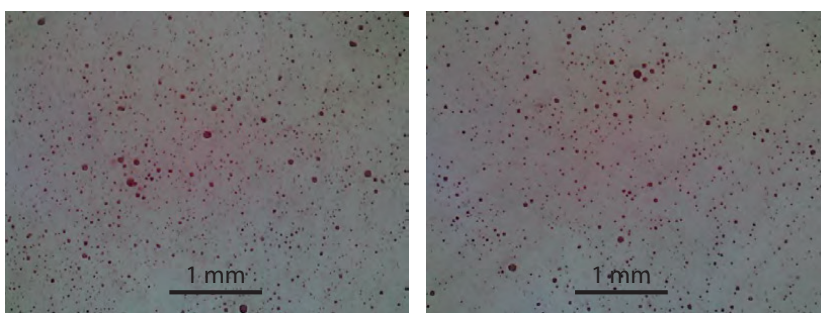


Figure 6: Pre-trial (control) sample images

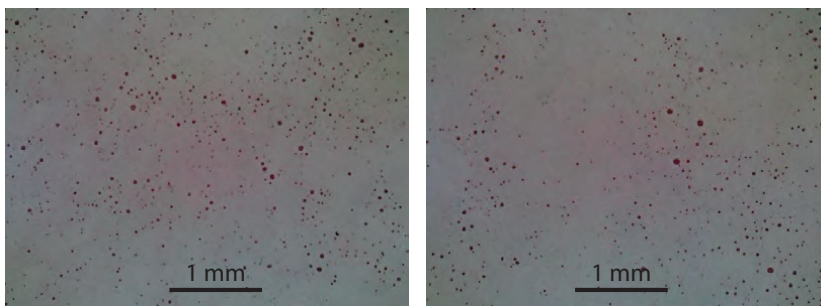


Figure 7: Trial starch sample images

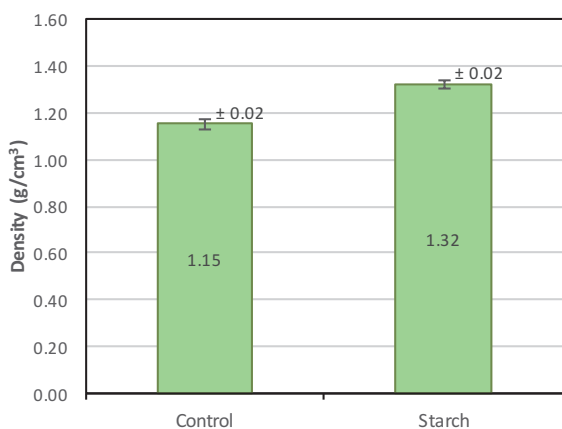


Figure 8: Density of control coating vs. starch coating, adapted from Schoenfelder (2017)

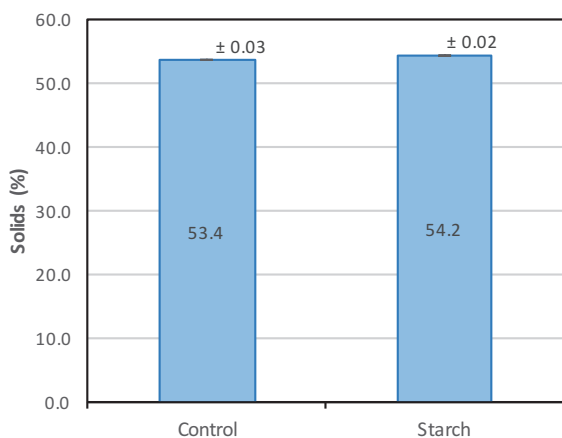


Figure 9: Solids of control coating vs. starch coating, adapted from Schoenfelder (2017)

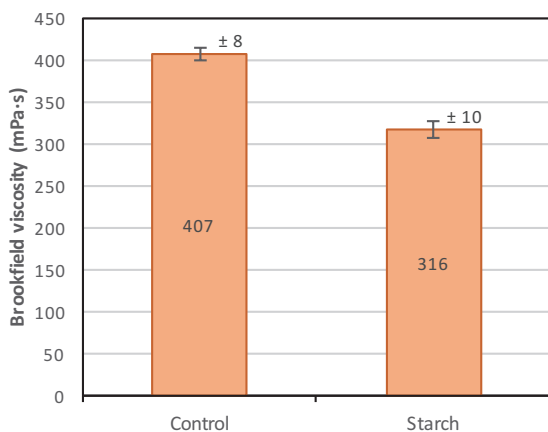


Figure 10: Brookfield viscosity of control coating vs. starch coating at 26.3 s⁻¹ shear rate

Through these results, one can see that the starch allowed for slightly higher solids (in %) and a higher density (in g/cm³) of the coating, but it's Brookfield

viscosity (at 26.3 s⁻¹ shear rate) was considerably lower than the original formula of control sample (Figure 10).

This might be attributed to the decreased thickener content, which may have increased viscosity (per part) more than the starch is capable of. The pH values of the coatings are not considerably different (data not shown, Schoenfelder, 2017), with the starch being slightly closer to neutrality than the control sample formula. This will not change the effect of the coating performance on the machine.

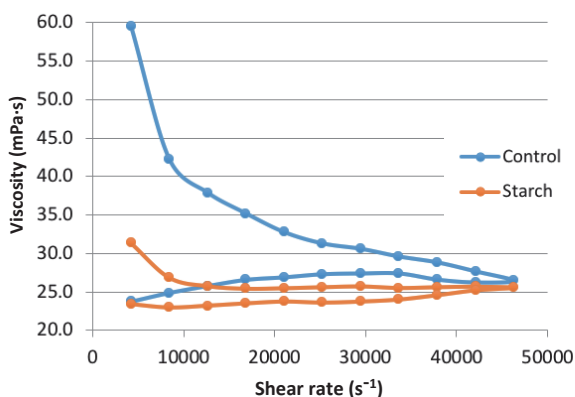


Figure 11: High shear viscosity vs. shear rate of the control coating and starch coating (Schoenfelder, 2017)

While both coatings show a pseudoplastic (shear-thinning) model curve, the control formulation has a higher initial viscosity (Figure 10), which quickly declines (Figure 11). This gives the control coating a larger area between the ramp up and the ramp down sections of the test; the area between the initial ramp up from 0 s⁻¹ to 46288 s⁻¹ and the final ramp back down to 0 s⁻¹ can help define how thixotropic a coating is – the larger the area the more thixotropic or shear thinning it obviously is (increased drop of viscosity). Thus, the control formulation is more thixotropic than the starch formulation. Low shear viscosity of coating colors usually reflects the viscoelastic region. Reducing the low shear viscosity by as much as 25 % has a large impact on converting the system from a strongly elastic rheology to a more viscous one. Such a move toward a more purely viscous system is known to prevent the elastic stretching and visible retention of coating color defects, such as bubbles.

The WRV measures how much water is released by a coating after drying. In theory, if water is held in by the coating instead of being released by drainage, there is a lower probability of the water creating air/vapor and bursting through the curtain coating layers during the drying process. Starch is hydrophilic in nature, and thus it is believed that the gravimetric WRV of the coating will decrease, as the coating will be able to hold on to more water.

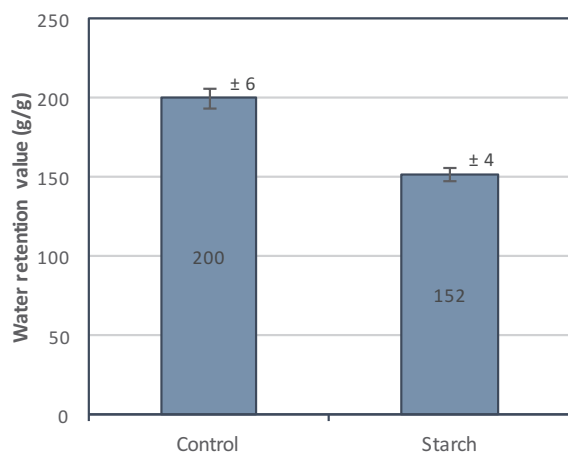


Figure 12: Water retention value (WRV) of control coating vs. starch coating (Schoenfelder, 2017)

Figure 12 shows the WRV results of the test on the control vs. the starch trial formulation. The results show improved water retention capabilities of the coating through the introduction of starch. It was found through lab trials that an increase of the starch content

within the coating batch did not help to lower the WRV any further, thus 150 g/g WRV seems to be where the starch's capabilities plateau. This significant drop from 200 g/g to 150 g/g WRV may help to decrease pitting, with water being held in the sheet and/or coating, not released through the coating. This also suggests that the formulation is less flocculated, and thus also less elastic.

4. Conclusion

The addition of starch to base and top coatings showed beneficial effects on decreased pitting area and size of pits. Addition of starch paired with decrease in the thickener addition resulted in decreased viscosity of the curtain coating. The viscosity was still around/above the 300 mPa·s range. Water retention levels of coatings seem to correlate with lower pitting – as the coating holds in more water, there is most likely less air passing through, which may be a mechanism for pit formation. The roughness of the base sheet (Table 3) might be adding to the overall pitting issue. The surface tension of the coating promoted increased wetting capabilities, but this did not affect pitting.

References

- BASF, 2016. *Surface Control*. [online] Available at: <https://www.dispersions-pigments.basf.com/portal/basf/ien/dt.jsp?setCursor=1_564555> [Accessed 8 May 2018].
- Becerra, M., and Carvalho, M.S., 2011. Stability of viscoelastic liquid curtain. *Chemical Engineering and Processing: Process Intensification*, 50(5–6), pp. 445–449. <https://doi.org/10.1016/j.cep.2010.11.011>.
- Birkert, O., Hamers, C., Krumbacher, E., Schachtl, M., Gane, P.A.C., Gerteiser, N., Ridgway, C.J., Fröhlich, U. and Tietz, M., 2006. Curtain coating of pigment coats. *Professional Papermaking*, 2, pp. 56–71.
- Brown, D.R., 1961. A study of the behavior of a thin sheet of moving liquid. *Journal of Fluid Mechanics*, 10(2), pp. 297–305. <https://doi.org/10.1017/S002211206100024X>.
- Chen, K.S., 1992. *Studies of multilayer slide coating and related processes*. PhD thesis. University of Minnesota.
- Chen, T., Joyce, M.K., Fleming, P.D., Lee, D.I. and Bloembergen, S., 2016. Pigmented formulations containing biobased nanoparticle binders for curtain coating applications; Part 1: Rheological study. In: *Paper Conference and Trade Show PaperCon 2016*. Cincinnati, Ohio, USA, 15–18 May 2016. Peachtree Corners, Georgia, USA: TAPPI Press.
- Döll, H., 2010. Curtain coating – wenn der Forhang fällt. *Wochenblatt für Papierfabrikation*, 138(6), pp. 483–488.
- Kistler, S.F., 1983. *The fluid mechanics of curtain coating and related viscous surface flows with contact lines*. PhD thesis. University of Minnesota.
- Klass, C.P., 2004. Is curtain coating ready for prime time? *Solutions!*, 87(12), pp. 30–32.
- Lee, H.L., Youn, H.J., Lee, K.H., Kim, C.H. and Kim, J.D., 2009. Development of new coated linerboard by combining condebelt drying and curtain coating technologies. In: *63rd Appita Annual Conference and Exhibition*. Melbourne, 19–22 April 2009. Carlton, Vic.: Appita, pp. 203–210.
- Liu, C.Y., Vandre, E., Carvalho, M.S. and Kumar, S., 2016. Dynamic wetting failure and hydrodynamic assist in curtain coating. *Journal of Fluid Mechanics*, 808, pp. 290–315. <https://doi.org/10.1017/jfm.2016.594>.
- Marston, J.O., Hawkins, V., Decent, V.P. and Simmons, M.J.H., 2009. Influence of surfactant upon air entrainment hysteresis in curtain coating. *Experiments in Fluids*, 46(3), pp. 549–558. <https://doi.org/10.1007/s00348-008-0580-7>.
- Owens, D.K. and Wendt, R.C., 1969. Estimation of the surface free energy of polymers. *Journal of Applied Polymer Science*, 13, pp. 1741–1747. <https://doi.org/10.1002/app.1969.070130815>.
- Pekarovicova, A. and Fleming, III, P.D., 2005. *Innovations in ink on paper technology to improve printability*. Surrey, UK: Pira International.

- Renvall, S., Kumar, V., Toivakka, M. and Salminen, P., 2013. Short time water absorption into multilayer curtain coated linerboard. In: *Paper Conference and Trade Show (PaperCon 2013): Volume 1*. Atlanta, GA, USA, 27 April–1 May 2013. Peachtree Corners, GA, USA: Tappi Press, pp. 192–212.
- Schoenfelder, S.L., 2017. *The Modification of a curtain coating formulation: a study of rheology and surface tension, and their effect on pitting*. Master's Thesis. Western Michigan University.
- TAPPI, 2005. *T 701 pm-01 Gravimetric method for measuring dewatering of coating colors (Abo-Akademi-type method)*. Peachtree Corners, GA, USA: TAPPI.
- Triantafillopoulos, N., Grön, J., Luostarinen, I. and Paloviita, P., 2004. Operational issues in high-speed curtain coating of paper, Part 2: Curtain coating of lightweight coated paper. *TAPPI Journal*, 3(12), pp. 1–16.
- Tripathi, P., 2005. *Stabilization of curtain coater at high speeds*. PhD dissertation. Western Michigan University.
- Tripathi, P., Joyce, M., Fleming, P.D. and Sugihara, M., 2009. A statistical study of process variables to optimize a high speed curtain coater – Part I. *TAPPI Journal*, 8(1), pp 20–26.
- Urscheler, R., Dobler, F., Roper, J., Haavisto, J. and Nurminen, T., 2005. Key attributes and opportunities of multilayer curtain coating for paper. In: *TAPPI Coating Conference and Exhibit*. Toronto, Ontario, Canada, 17–20 April 2005. Norcross, GA, USA: TAPPI Press.



TOPICALITIES

Edited by Markéta Držková

CONTENTS

News & more	179
Bookshelf	181
Events	187

News & more

A yearly update on ISO standards for graphic technology

Among the standards under the direct responsibility of ISO technical committee TC 130 Graphic technology, there are currently 35 standards under development, with three in the approval stage. The standards reconfirmed during the last year are ISO/TS 10128:2009 Graphic technology – Methods of adjustment of the colour reproduction of a printing system to match a set of characterization data, all four parts of ISO 12637 Graphic technology – Vocabulary, i.e. its Part 1: Fundamental terms (from 2006), Part 2: Prepress terms (2008), Part 3: Printing terms (2009) and Part 4: Postpress terms (2008), and ISO 12640-5:2013 Graphic technology – Prepress digital data exchange – Part 5: Scene-referred standard colour image data (RIMM/SCID), specifying a set of standard colour image data encoded according to the Reference Input Medium Metric RGB specification, while the standards reviewed and confirmed for the first time include two parts of ISO 12647 Graphic technology – Process control for the production of half-tone colour separations, proof and production prints – Part 1: Parameters and measurement methods and Part 3: Coldset offset lithography on newsprint (both from 2013), ISO 14298:2013 Graphic technology – Management of security printing processes, and ISO 15397:2014 Graphic technology – Communication of graphic paper properties. The recently published standards and technical specifications are briefly introduced in the following parts.

ISO/TS 15311-1:2019 and ISO/TS 15311-2:2018

Graphic technology – Print quality requirements for printed matter

Part 1: Measurement methods and reporting schema

Part 2: Commercial print applications utilizing digital printing technologies

The revised and extended second edition of the first part of this technical specification was published in February 2019, replacing the first edition from 2016; now it is again under review, with a new version being developed. It defines print quality metrics, measurement methods and reporting requirements for printed sheets, primarily from digital printing systems. Their application for assessing printed products on isotropic substrates that are typically held at a viewing distance of 30 to 50 cm is specified in the second part, which was first published in October 2018.

ISO 16684-1:2019

Graphic technology – Extensible metadata platform (XMP)

Part 1: Data model, serialization and core properties

The first version of the standard from 2012 was revised and published this April as a second edition. It deals with the Adobe's Extensible Metadata Platform introduced in 2001 and specifies the XMP data model, defining the forms of XMP metadata items, the serialisation of XMP that defines how any instance of the XMP data model can be recorded as XML (eXtensible Markup Language), and a collection of core XMP metadata items. While the standard was prepared by TC 130 Graphic technology, it is now under the responsibility of TC 171/SC 2 Document file formats, EDMS systems and authenticity of information (the same applies for the second part of ISO 16684).

Paperbase evolution in 2018

paperbase INTERNATIONAL

Since last year, Paperbase has a new supplier

and due to some downtime from July to October the numbers of records added during 2018 are lower across all categories. The total growth still exceeded five thousand entries and the number will increase by about two thousand for 2018 publications, mainly from non-English literature.

Comparing to the records added during 2017 (see the News & more section in 7(2018)2), there is higher diversity in the numbers across the subject areas. Again, the most represented are composites, wood and wood chemistry, nanocellulose, and non-wood fibrous raw material. Production and recovery of cooking chemicals, pulp industry by-products and biorefining, properties and testing of finished paper and board, paper, board and nonwoven packaging, as well as technical aspects of company information, are also above the third quartile. While in 2017 new records in these areas comprised 33 % of the total, in 2018 it was 57 %.

When looking at the statistics of Paperbase searches, the number of words used in queries as well as the overall number of searched words were at first more or less the same as in 2017 and then they approximately doubled in the second half of 2018. Besides the general terms from the field, with cellulose, fibres, paper and pulp at the top of the list, the queries reflect the high interest in biomaterials and bioprocesses, nanofibres and microfibrils (all with hundreds of searches). Further, the frequently searched concepts include biomass, creep, extraction, moisture, sorption, starch, whiskers, and also conferences and symposia.

We thank Camilla Burman, RISE Research Institutes of Sweden, for providing the Paperbase data.

News from drupa

In August, the 2nd drupa Global Trends Spotlight was published, this time focused on the topic of systems integration. The report was prepared by



Printfuture (UK) and Wissler & Partner (Switzerland),

based on the specific survey completed by over 500 printers and 150 manufacturers and suppliers. According to the results, two-thirds of the surveyed companies use some prepress workflow solution. Colour management workflow, job scheduling, financial package, and MIS (Management Information System) or ERP (Enterprise Resource Planning) software are used by 50 % or more printers. The least used, by less than 25 %, are solutions for JDF (Job Definition Format) workflow and Web-to-Print or digital storefront.

When looking at the progress on integration, the larger the company, the more progress is reported. While printers see the biggest challenge in the sheer complexity and scale of the project, in the view of suppliers it is the lack of awareness of the importance of the issue by customers.

On the other hand, both printers and suppliers identified reducing errors, wastage and quality costs as the main benefit observed. Among the obstacles, insufficient resources and the lack of skills or specialist knowledge were the most listed reasons for making no progress at all.

For a majority of printers, systems integration is an important priority. Concerning a software licensing model, over 70 % of printers still prefer to buy a software licence rather than to pay for an online SAAS (software-as-a-service) solution, which is reflected in suppliers' offer.

Since the beginning of September, the exhibitor database for drupa 2020 is online and the Ticket shop is open, offering discounted conditions and free public transport access. Also, the drupa world tour that presents the fair together with the most important trends and innovations in the industry started in Mexico City and will continue until spring 2020.

ISO 19302:2018

Graphic technology – Colour conformity of printing workflows

This new standard published in December 2018 is applicable to any printing process using any colourant and defines the requirements of printing workflows and evaluation methods for their tone and colour reproduction.

ISO 20294:2018

Graphic technology – Quantification and communication for calculating the carbon footprint of e-media

This new standard available since November 2018 is based on a life cycle assessment approach and specifies the requirements for quantifying the carbon footprint of processes, materials and technologies that are necessary for e-media archiving, distribution, use and storage.

ISO 20677:2019

Image technology colour management – Extensions to architecture, profile format, and data structure

Building on ISO 15076-1 that defines the architecture, profile format and data structure based on ICC.1:2010, this new standard from February 2019 describes an expanded profile specification and profile connections that permit greater flexibility and functionality, with some ISO 15076-1 types removed and others added. A colour management module compatible with profiles conforming to this document will have backwards compatibility with those conforming to ISO 15076-1. Additional workflow requirements and restrictions are defined in interoperability conformance specifications approved and registered by the International Color Consortium (ICC).

ISO 21632:2018

Graphic technology – Determination of the energy consumption of digital printing devices including transitional and related modes

This new standard from December 2018 defines how to measure and calculate the electricity consumption of digital production press in the cases when it is significantly influenced by its modes other than production printing mode. It can be used to compare the energy efficiency figures for different machine set-ups, such as the best-quality or highest-productivity ones.

ISO 21812-1:2019

Graphic technology – Print product metadata for PDF files Part 1: Architecture and core requirements for metadata

Published this June, this new standard defines the document part metadata in a PDF file that can be used to communicate the intended appearance of print products and their components. It builds on the DPart syntax as specified in ISO 16612-2 (PDF/VT) and ISO 32000-2 (PDF 2.0).

ISO/TS 21830:2018

Image technology colour management – Black point compensation for n-colour ICC profiles

This short technical specification available since September 2018 specifies a procedure for extending the black point compensation method described in ISO 18619:2015 for either CMYK colourants plus combinations from the defined set or CMY-like chromatic colourants with widely-spaced hue angles.

Bookshelf

Multisensory Packaging: Designing New Product Experiences

Product packaging, which had not seen any substantial development over many decades, has recently received increased attention from both academic researchers and packaging practitioners for many reasons. From a marketing perspective, it is mainly thanks to a growing understanding of the human mind and senses on the one hand, and new technologies enabling to enhance user experience on the other hand. The authors and editors of this book consider the important aspects of packaging and explore the transformation of the way in which the packaging is designed and interacted with, including a number of case studies and examples of multisensory perception.

After the introduction of the topic, the content is organised into three parts. The first one explains the role of main packaging characteristics, from its colours, imagery, transparency and typefaces stimulating the eyes, up to the less obvious ones, such as the sounds produced when the consumer interacts with product packaging and the tactile attributes experienced during haptic interaction with the packaging.

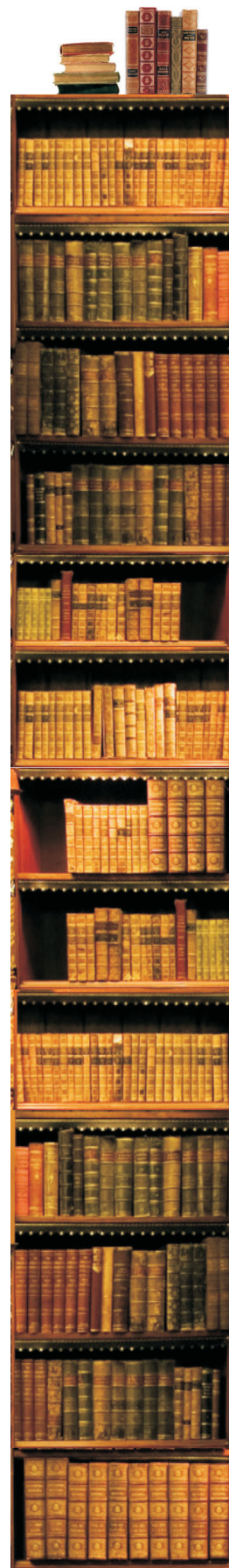
The second part then discusses multisensory packaging frameworks and contexts. It starts with the origins of product perception and sensory evaluation according to the embodied cognition framework, discussing the influence of design variables relating to the shape, graphic layout, composition and tactile properties of packaging, as well as the influence of their interplay and matches between expectations generated by packaging design and sensory impressions on experiencing the product. Next, the various approaches to facilitate efficient multisensory design innovation are reviewed, outlining a novel framework for the multisensory analysis of product packaging and stressing the importance of congruency. Two chapters then investigate whether and how the multisensory packaging design can communicate food health benefits to consumers and express premium quality, with the following one focused on the impact of individual and cultural differences.

Finally, the third part deals with the two fields of research most relevant for the future of multisensory packaging. First, concerning the use of consumer neuroscience in the optimisation of multisensory packaging, the possible applications of neuroimaging techniques for packaging research in order to understand the response of consumers and even to predict a product's sales success are discussed, identifying the key challenges and limitations. Second, the recent development of sensory-enabling technologies originated mainly from research into human-computer interaction is presented together with the possibilities of their incorporation into the packaging of different products to deliver novel multisensory experiences, with the focus of various augmented reality solutions.



Editors: Carlos Velasco, Charles Spence

Publisher: Palgrave Macmillan
1st ed., November 2018
ISBN: 978-3-319-94976-5
378 pages, 26 images
Hardcover
Available also as an eBook



Document Image Processing for Scanning and Printing

Authors: *Ilya V. Safonov, Ilya V. Kurilin, Michael N. Rychagov, Ekaterina V. Tolstaya*

Publisher: Springer
1st ed., March 2019
ISBN: 978-3030053413
305 pages, 249 images
Hardcover
Also as an eBook



This book presents the main results of the authors' studies and their recent work for the industry. In the development of the algorithms, the emphasis was put on low computational complexity and model size, allowing their implementation on embedded platforms. The book deals with distortion-free scanning and copying of bound documents, document image enhancement, memory-efficient two-sided copying, automatic cropping and de-skew of multiple objects, scanned newspapers and magazines segmentation, document image classification based on layout information, scanning and stitching of large originals, fast control of JPEG compression rate, scanned text vectorisation, screenshot to metafile conversion for printing, embedding digital hidden data into hardcopy, on-the-fly microtext generation, micropictures for copy protection, toner saving by random perforation, and integral printing of 3D images. The book 'Adaptive Image Processing Algorithms for Printing' of the same authors is also available.

Physical Testing of Paper

Author: *Roman E. Popil*

Publisher: Smithers Pira
1st ed., December 2017
ISBN: 978-1910242926
230 pages, 94 images
Softcover
Also as an eBook



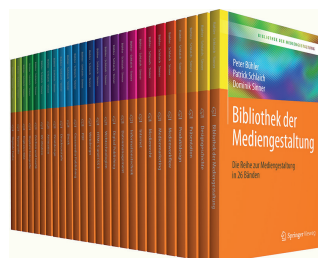
The author of this book shares his expertise in the development and practical use of the methods for paper characterisation. After introducing the very basics of paper structure

Bibliothek der Mediengestaltung: Die Reihe zur Mediengestaltung in 26 Bänden

All 26 volumes of this comprehensive series on media design published during 2017–2019 for the German-speaking readers are now available as one set. It is also possible to buy one of the four subsets focused on design and media technology, media design, print media or digital media, each consisting of seven volumes. The library builds upon the successful compendium on media design (sixth edition of which was published in 2014 in four volumes). For the current series, the topics are restructured into more volumes in a handy format, each having about one hundred pages. The content covering the knowledge in both print and digital media and design has been completely revised to include the latest industry developments. All volumes are intended as textbooks and workbooks for education in the field at both high-school and college levels, as well as for self-study. The concise but detailed content is accompanied by numerous illustrations and practical tasks with detailed solutions.

The series opens the volume on visual communication, introducing the communication models, visual perception, basic design rules and elements, perspective and colour. Seven volumes then deal with different aspects of content creation, from digital colour with colour design considerations, colour management and processing, over typography (type technology, design and readability), digital images – their use in design, editing and processing, and digital photography, describing image capture, optics and camera technology, up to signs and graphics (logos, infographics and 2D/3D graphics), audio and video media covering film design and audio/video technology, and animation with basic concepts and examples of 2D and 3D animation.

Three volumes are focused on print media. The one on print design introduces design techniques, layout principles, page design, print products and advertising media. The volume on prepress describes text, graphics and image data processing from data acquisition and transfer to the output for professional printing, while the one on printing provides the basics of the different printing, postpress and finishing processes together with the materials used. Another two volumes deal with cross-media publishing – the media-neutral data, XML, Web-to-Print and PDF-to-Web, and PDF – the basics of the format and production of print or interactive PDF files. There are also volumes on web design for interfaces, screens and mobiles, HTML5 and CSS3 specifications for multimedia and responsive websites, web technologies (JavaScript, PHP language and databases), digital publishing – eBooks, content management systems and applications, data management (data, databases and data security), information technology (hardware, software and networks), and internet – the technology, use and social media. The remaining volumes cover media law, media marketing – branding, advertising and corporate identity, media workflow with costing and project management, presentation design, product design, and history of design.

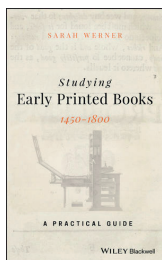


Authors: *Peter Bühler, Patrick Schlaich, Dominik Sinner, Andrea Stauss, Thomas Stauss*

Publisher: Springer
1st ed., April 2019
ISBN: 978-3-662-59318-9
2665 pages, 5063 images
Softcover
Individual volumes available also as eBooks

Studying Early Printed Books, 1450–1800: A Practical Guide

The guide provides a profound insight into the technologies and practices of hand-press printing to help understand how early printed books were made and how it influences the way they are read and understood today. In the first part, the author describes the steps of making a book and also considers the economics of printing. The second part then deals more in-depth with paper, type, format, printing, corrections and changes, illustrations and binding, while the third one provides details about individual typographic elements on the page in alphabetical order. Namely, it describes advertisements, alphabet and abbreviations, blanks, dates, imprint statements (followed by an explanation of the vocabulary for different versions – edition, impression, issue, state, copy), initial letters, marginal notes, music, pagination and foliation, preliminary leaves, press figures, printer's devices, printer's ornaments, privileges, approbations and imprimaturs, signature marks, title pages, and volvelles and movable figures. The fourth part explains how to examine a book, introducing good research habits and handling books, how to look at their appearance, contents, page features and usage, and also specifics in the case of working with digitised images. The fifth part shows how to differentiate between early modern elements and the parts altered during the existence of a book.



Author: Sarah Werner

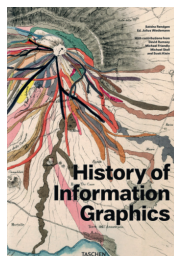
Publisher: Wiley-Blackwell
1st ed., February 2019
ISBN: 978-1-119-04997-5
216 pages
Hardcover
Available also as an eBook

History of Information Graphics

This large compendium with six fold-outs shows the evolution of data visualisation through the selection of significant works across different fields, such as astronomy, cartography, zoology and technology, including famous examples as well as the almost unknown ones. After the introductory essay, the four main parts deal with the medieval period, early modern period, 19th century and 20th century, providing historical and cultural contexts of each work. The book also offers the contributions on the special historical collections – 'Seeing data through maps' by David Rumsey, 'Mining gems from the history of data visualization' by Michael Friendly, 'Understanding humans and machines' by Michael Stoll, and 'The forgotten origins of news infographics' by Scott Klein.

Author: Sandra Rendgen

Publisher: Taschen
1st ed., July 2019
ISBN: 978-3-8365-6767-1
462 pages
Hardcover



and properties, the chapters explore tensile properties, ultrasonic testing, bending stiffness of paper and corrugated board and its connection to caliper and tensile stiffness, compression testing of paper, board and boxes and its relationship to tensile testing, elastic modulus and the influence of artefacts, testing methods for measurement of the writability and printability of papers, and the so-called beater curves to evaluate pulp potential, namely the burst index and tear index.

Early Music Printing in German-Speaking Lands

Editors: Andrea Lindmayr-Brandl,
Elisabeth Giselbrecht, Grantley McDonald



Publisher: Routledge
1st ed., March 2018
ISBN: 978-1138241053
290 pages
Hardcover
Also as an eBook

This book brings an in-depth look at the music printing and publishing in the 15th century along with the problems and solutions concerning printing techniques and explores the relationship of music printing and commerce, as well as its place in intellectual history. The text is illustrated with plates, tables, music examples and numerous figures with geographical information, types, title pages, watermarks, etc.

The Aries Press of Eden, N.Y.

Author: Richard Kegler



Publisher: RIT Press and
Wells College Press
1st ed., December 2018
ISBN: 978-1939125224
96 pages, 39 images
Hardcover

This deluxe edition of the book on the American private press that was founded by Spencer Kellogg, Jr. in the 1920s and produced exceptional examples of fine printing features additional pages, such as an original leaf from *The Ghost Ship*.

Fundamentals of 3D Food Printing and Applications

Editors: *Fernanda C. Godoi, Bhesh R. Bhandari, Sangeeta Prakash, Min Zhang*

Publisher: Academic Press
1st ed., November 2018
ISBN: 978-0128145647
728 pages, Softcover
Also as an eBook

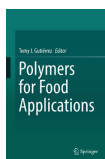


After an introduction to the principles of 3D food printing, the book details the available technologies and factors affecting printing precision, as well as the critical variables. Then is explored the printability of several materials, including the cereal-based and insect-enriched printable food, 3D-printed food from fruits and vegetables, potential 3D printing applications of dairy products, and 3D chocolate printing. The book also deals with the creation of food structures through binder jetting, domestic applications of 3D food printing technology, the role of digital platforms in prosumer-driven 3D food printing, as well as the safety and labelling of 3D-printed food. It concludes with the future outlook of 3D food printing.

Polymers for Food Applications

Editor: *Tomy J. Gutiérrez*

Publisher: Springer
1st ed., August 2018
ISBN: 978-3319946245
818 pages, 161 images
Hardcover
Also as an eBook

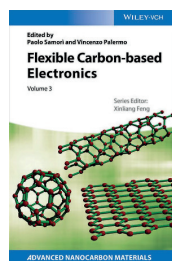


With almost 70 contributors, this exhaustive review presents the polymer-based systems for food applications – from various edible films, coatings, foams, gels and emulsions, over polymers for food packaging, up to the methods of nano- and microencapsulation, along with the role of different polymers in the development of gluten-free baked goods, perspectives on 3D food printing, and also the sensors based on conducting polymers for the analysis of food products.

Flexible Carbon-based Electronics

According to the editors of this book published as the third volume of the Advanced Nanocarbon Materials series, the future of carbon-based materials for electronic applications requiring flexible components seems very promising, in contrast to high-speed, conventional electronics applications, where the probability of displacing silicon is very low. Contributed by leading scientists working in this research field, the book deals with the materials, processes and main applications, stressing the importance of the structure-function relationship for the target-oriented fabrication.

There are two chapters introducing different types of soft composites with tunable optical and electrical properties and organic semiconductors for transparent electronics, as well as the chapter on the processing of graphene and its applications for flexible electronics. Another chapter is focused on the characterisation of graphene flexible materials and displays. One chapter is dedicated to the printing of 2D materials. It provides an overview of suitable coating and printing techniques, describes formulation and characterisation of electronic inks, processing steps from exfoliation of layered crystals, over stabilisation of exfoliated flakes and ink formulation, up to printing and coating of 2D-crystal-based inks, as well as the applications for printed electronics and optoelectronics, sensors and wearable devices, energy devices and printed THz devices. The remaining chapters explore flexible solar cells, development of organic field-effect transistors for operation at high frequency, display technology and applications based on active-matrix organic light-emitting diodes (AMOLEDs), flexible batteries, and flexible organic bioelectronics and biosensors.



Editors: *Paolo Samori, Vincenzo Palermo*

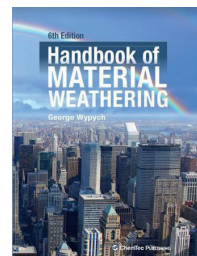
Publisher: Wiley-VCH
1st ed., February 2019
ISBN: 978-3-527-34191-7
336 pages
Hardcover
Available also as an eBook

Handbook of Material Weathering

Based on the thorough review of published papers, patents and other relevant sources, the 6th edition of the handbook provides a comprehensive summary of the current knowledge on material weathering. It is organised into 22 chapters, going from photophysics and photochemistry, over measurement conditions, methods and interpretation, to information on weathering of different types of materials, including biodegradation.

Author: *George Wypych*

Publisher: ChemTec Publishing
6th ed., March 2018
ISBN: 978-1-927885-31-4
972 pages, 807 images
Hardcover



Bookshelf

Academic dissertations

Print and Screen, Muriel Cooper at MIT

This dissertation is the first dedicated to Muriel Ruth Cooper (1925–94), who worked at MIT (Massachusetts Institute of Technology) as a graphic designer, an educator and a researcher. The dissertation outlines her background, education and early jobs and then in four chapters reviews more than four decades of her career at MIT, presenting her significant contributions in both print and digital media. The work of Muriel Cooper for MIT started when she became the first in-house designer of the Office of Publications, established in the early 1950s. Her approach is well illustrated by the fact that when designing flyers for the summer session courses, she consulted the instructors to understand the material better and to find suitable artwork – in order to make the language of science more intelligible. Further, the first chapter considers some of her teaching and freelance work in the years around 1960, including the design of a graphic identity for the MIT Press. The second chapter begins with 1967 when Muriel Cooper joined the Press full-time as its first Design and Media Director and began work on the book about the Bauhaus. Besides individual titles, she designed publishing processes – routing and tracking systems as well as standardised formats and typography, while increasingly using software to streamline the workflow. The chapter also deals with the controversy during the design of the book *Learning from Las Vegas*. The next one is dedicated to Cooper's role as a teacher of experimental printing within the Visible Language Workshop, founded in 1974. Finally, the fourth chapter explores her work at the MIT Media Lab, proposed as a facility for interdisciplinary research on motion pictures, print, computing arts and media technology, since 1985 until her death. The dissertation also mentions colleagues of Muriel Cooper and her relations with contemporary graphic designers. The images illustrating her life and work were selected from the related archives and collections, mostly from the Muriel R. Cooper Collection, and are presented in the appendix.

3D Printed Bone-Like Biopolymer Composites Inspired by Nacre

The research within this thesis was aimed towards the prospective load-bearing bone grafts, namely the fabrication of 3D composites of chitosan and calcium carbonate with suitable properties. This approach comprising the development of a nacre-like material was expected to be more straightforward than replicating bone, while the mechanical strength of nacre and bone is comparable and mostly attributed to their respective composition and nanostructure. The work utilised the described method of a synthetic biomineralisation, developed to replicate the elements of nacre's nanostructure in 2D biopolymer systems in laboratory conditions, and investigated its applicability for the mineralisation of 3D-printed scaffolds based on chitosan hydrogel with calcium carbonate.

To develop the desired 3D structures with interconnected macropores, the custom-designed 3D printer enabling to print a variety of liquid materials was used. It was based on the open-source MendelMax 2.0 by Maker's Tool Works, with custom-built syringe extruders and a heated fan attachment. First, it was necessary to test the printer, verify the applicability of chitosan

Doctoral thesis – Summary

Author:
Robert Wiesenberger

Speciality field:
Art and Design History

Supervisor:
Barry George Bergdoll

Published:
6 April 2018,
Department of Art History and
Archaeology, Graduate School of Arts
and Sciences, Columbia University
New York, New York, United States

Contact:
rwiesenberger@clarkart.edu

Doctoral thesis – Summary

Author:
Mima Kurian

Speciality field:
Chemistry

Supervisors:
Kathryn McGrath
Ross Stevens

Defended:
2 July 2018, Victoria University
of Wellington, School of Chemical
and Physical Sciences
Wellington, New Zealand

Contact:
mima.kurian@vuw.ac.nz

hydrogels as the printing ink and characterise its rheology, find the printing parameters allowing to fabricate a stable 3D porous scaffold and test the techniques used to dry the as-fabricated scaffolds, as well as to study their effects on the scaffold properties and swelling behaviour. The next step concerned the process of mineralisation of the 3D scaffolds, elucidating the required strategies including the use of polyacrylic acid as a crystal growth modifier. By modulating the period of exposure to the mineralisation solutions and their concentrations, it was possible to fabricate 3D composites with up to 40 % calcium carbonate content and varying crystal morphology. It was observed that the calcium carbonate crystallites were intricately associated with the organic hydrogel matrix. Further, the alternative single-step method using chitosan hydrogel preloaded with calcium carbonate crystallites as the printing ink was investigated. Based on the comparison of the advantages and disadvantages of both methods it was found that the two-step fabrication method is superior in terms of the properties explored and desired in the composite. Throughout the thesis, the analyses employed a number of characterisation methods. For air-dried scaffolds and composites, the compressive modulus, strength and indentation hardness values obtained were within the same order of magnitude as that of trabecular bone. The work also discusses the effect of mineralisation and its extent, as well as of the morphology and size of the resultant crystallites, on the mechanical properties. Finally, the capacity of fabricated 3D composites to enable osteoblast cell attachment and proliferation was confirmed.

Doctoral thesis – Summary

Author:

Sofia Thorman

Speciality field:

Chemical Engineering

Supervisors:

*Li Yang
Magnus Lestelius*

Defended:

*18 December 2018, Karlstad
University, Faculty of Health, Science
and Technology, Department of
Engineering and Chemical Sciences
Karlstad, Sweden*

Contact:

sofia.thorman@ri.se

Where Did the Ink Go?

The Effect of Liquid Absorption on Ink Distribution in Flexography

The topic of this thesis was the distribution of ink on coated paper and board substrates, particularly the impact of the substrate liquid absorbency in the flexographic printing and its contribution to an uneven ink distribution. The research included the experiments on a monochrome area, where the ink interacted directly with the substrate, as well as on a polychrome area, where the overprinted ink interacted with the previously printed ink layer rather than with the substrate surface. As the print non-uniformity can be to a large extent influenced also by surface roughness, the care was taken to separate its effects from that of coating layers absorbency using the systematic approach and proper selection of materials. The substrates included pilot-coated boards and fine papers, in some cases with absorption-modified surfaces, as well as commercially produced boards. The work employed flexographic printing with water-based inks at 0.5 ms^{-1} in laboratory scale (one-colour) and at 7 and 10 ms^{-1} in production scale (for both one-colour and overprinted samples, with the first ink layer applied using two anilox rollers with different volume). To characterise absorption non-uniformities, a new staining technique was developed. Its applicability was tested also for water-moisture interference issues in production sheet-fed offset printing. It was shown that low liquid absorption increases the risk of uneven print; the coating layers with small pores and low liquid uptake generated higher print mottle, attributed to high flow resistance in pressure-driven liquid absorption. For the absorption-modified surfaces, the areas with compact pore structures hindered ink penetration and caused brighter spots in the print. To study the ink trapping mottle, another new technique combining scanner and microscopy analysis was introduced to quantify the non-uniformities in the overprint layer. The results show that an uneven distribution of the first ink causes unevenness of the overprint layer – the thinner the bottom layer, the thicker the upper one. In addition, too slow or uneven ink absorption made ink trapping more sensitive to printing speed.

Events

PRINT 19

Chicago, Illinois, USA
3–5 October 2019



This year the event of the Association for Print Technologies (APTech) opens the keynote presentation 'The Wired Future' by Nicholas Thompson, discussing the main aspects of the changes coming due to the use artificial intelligence and robotics, increasing interconnectivity and dominance of global technology corporations – and how can the media continue upholding the truth throughout. The exhibition highlights the newest products recognised as the RED HOT Technology and offers the TechWalk tours guiding visitors who need an overall show-floor overview or who are interested in label and packaging, substrates, metallic print decorating options, inkjet, workflow solutions or the balanced scorecard approach to strategic performance management. The programme also includes TechTalk panel sessions hosted by manufacturers and dealing with different topics, from the use of smartphones for colour measurement (instead of spectrophotometers), expanded gamut and special colours, including metallic, neon and digital ones, workflow and mailing solutions, data quality, software and PDF, over inkjet technology, direct-to-garment printing, wide-format printing, digital packaging, finishing, consumables, inks, paper and other substrates, up to the new print business opportunities. More than 60 other learning sessions covering various areas are scheduled, including hands-on courses.

RadTech Europe 2019

Munich, Germany
15–16 October 2019



The European edition of this conference and exhibition dedicated to the ultraviolet and electron-beam (UV/EB) curing technology brings the two-day programme with three or four parallel tracks, combining oral presentations with end-user and education sessions, complemented by poster presentations and new product introductions in the tabletop area.

The end-user sessions are focused on food packaging and metal coating, while the full-day training introduces the market, raw materials, chemistry and formulation, curing equipment and manufacturing. The lecture sessions cover the development and advances in photopolymerisation in composite materials, raw materials for UV and EB processes, including sustainable raw materials, radiation-curable coatings and adhesives, 3D printing with UV technology, measuring and monitoring in UV and EB processes, EB and UV LED systems for printing and packaging, UV LED photoinitiators and applications, and photopolymerisation chemistry. The contributions connected to printing deal, for example, with the effect of new acrylate resins on impact strength in 3D printing, or the development of low-voltage EB equipment to meet the challenges of the fast-growing packaging market.

GPC Print Media Conference 2019

Richmond, Virginia, USA
2–3 October 2019



For this year's edition, the conference is co-located with the Technical Forum of the Gravure Association of the Americas to expand the value to both end-users and suppliers. The joint sessions comprise an update on the economic situation and outlook and the 2019 Golden Cylinder Awards. The conference programme covers current legislation changes, supply chain logistics, market outlook for gravure publishing papers, a campaign promoting the sustainability of print and paper, education in the field at the University of Wisconsin-Stout, and more.

Digital Print Europe 2019

IMI EUROPE Berlin, Germany
7–10 October 2019

This event held by the IMI Europe starts with two days of the Inkjet Academy, followed by two days of the Digital Printing Conference. In addition, the market and technology forum on digital packaging printing takes place in the morning and the forum on mergers and acquisitions in the afternoon on the second day.

51st Conference of the International Circle of Educational Institutes for Graphic Arts Technology and Management

Tashkent, Uzbekistan
8–12 October 2019



In 2019, the IC conference is hosted by the Department of Textile and Light Industries of the University of Tashkent.

PrintIstanbul 2019 3rd International Printing Technologies Symposium

Istanbul, Turkey
10–12 October 2019



In 2019, this biennial symposium organised

by the Marmara University (not to be confused with the event of the same name held at the Istanbul University, see the Events section in 7(2018)3) again combines the talks in English and in Turkish. Their topics range from gravure and flexography printing of highly conductive reduced graphene oxide inks, formulation of silver–graphene hybrid conductive ink and fabrication of microcapsules for thermochromic inks, over a new design of pH-responsive packaging materials, pyrolysis characteristics of corrugated basepaper and characterisation of functional coatings with fragranced microcapsules, to a compensation method for tone value changes, machine learning algorithms in digital halftoning and image manipulation limits, to name a few.

ICGIP 2019 11th International Conference on Graphics and Image Processing

Hangzhou, China
12–14 October 2019

This year's edition of this event held mainly in Asia



features the keynotes presenting the optical scanning holography, i.e. a single-pixel real-time digital holographic recording technique, and applications of deep learning algorithms to image understanding and 3D shape editing, among others.

PRINTING United 2019

Dallas, Texas, USA
23–25 October 2019

Built on the SGIA Expo, this new event extends also



into the commercial, packaging and in-plant printing segments.

2019 NPIRI Fall Tech Conference



Oak Brook, Illinois, USA
15–17 October 2019

The conference organised by the National Printing Ink Research Institute (NPIRI) under the auspices of the National Association of Printing Ink Manufacturers (NAPIM) includes sessions focusing on technical, regulatory and new technology topics. The programme for this year again starts with the half-day pre-conference short course introducing to ink formulation and manufacturing. In the afternoon, the conference is opened by Dave Sullivan's keynote looking at communication through the lens of neuroscience, followed by the talks presenting the sustainability issues from a printer's perspective, the industry projects of students from Ryerson University and the state of the industry. The first day closes with the supplier showcase and tabletop exhibitions. The technical sessions on the second day cover paper substrates, carbon black, dispersion technology, colour measurement and UV LED technology; the regulatory ones then deal with the TSCA (Toxic Substances Control Act), OSHA (Occupational Safety and Health Administration) compliance, current supply chain issues, smart manufacturing and global compliance. Same as last year, the new technology session on the third day is shared with the Electronic and Conductive Ink Conference sponsored by NAPIM and Rodman Media, see below.

Electronic and Conductive Ink Conference 2019

Oak Brook, Illinois, USA
17–18 October 2019



Electronic and Conductive Ink
CONFERENCE

This technical conference that was successfully launched last year aims to highlight the different types of inks, including those based on silver, copper, carbon nanotubes and more, their deployment by equipment manufacturers, as well as the needs of the end-use customers. The 2019 programme features a keynote talk 'The technologist's guide to printed electronics' by Erika Rebrosova, sessions presenting new technology and technical talks session, all complemented by tabletop exhibitions.

CIC27 – 27th Color and Imaging Conference Color Science and Engineering Systems, Technologies, and Applications



Paris, France
21–25 October 2019

The Society for Imaging Science and Technology in cooperation with the related national and international organisations traditionally offers a week of courses, workshops, paper presentations, exhibits and conversations on colour and imaging topics, this year in Europe. For the third time, the International Symposium on Multispectral Colour Science is co-located with CIC; the oral presentations of its 20th edition are scheduled at the end of the conference. Another co-located event is the one-day Material Appearance Workshop that is organised by APPA-MAT, one of the research groups of CNRS, the French National Centre for

Scientific Research. The four workshop sessions are scheduled on Monday, with contributions on appearance measurement and characterisation, materials, reproduction and rendering, as well as with short talks and poster introductions. The keynotes opening each session are ‘Traceability and references for the measurement of appearance’ by Gaël Obein, ‘Reproducing images: colour and texture’ by Carinna Parraman, ‘Appearance analysis of fluorescent objects’ by Shoji Tominaga, and ‘Multi-material 3D printing for appearance fabrication’ by Vahid Babaei.

From 15 short courses offered on the first two days of CIC27, two has been revised (dealing with spatial colour perception and image processing and with advanced colorimetry and colour appearance) and three are new, focused on vector space arithmetic for solving colour problems, digital cinema environment and image quality evaluation, and colour imaging challenges with compact camera optics. In addition, four workshops can be attended on Tuesday; their topics comprise future directions in image quality, lighting and chromatic adaptation, the high-end digital colour print-making, and cultural heritage digitalisation. The technical programme then consists of over 30 oral and 40 interactive papers (posters), with each day opened by the keynote talks given by Marina Zannoli, presenting the perception-centred development of near-eye displays for augmented and virtual reality, Andrew Watson, describing the efforts to extend the simplified model of the spatio-temporal luminance contrast sensitivity function (the so-called pyramid of visibility) to the chromatic domain, and Panagiotis-Alexandros Bokaris exploring the challenges of video-projected augmented reality systems.

SecurityPrinters 2019

SecurityPrinters **COPENHAGEN** 23–25 Copenhagen, Denmark
Banknotes+Identity **HAGEN** 10/2019 23–25 October 2019

This conference with the exhibition is organised by Intergraf and open exclusively to security printers, their suppliers and postal, banknote issuing, government and law enforcement authorities. To guarantee neutrality and objectivity, it is not sponsored. In 2019, the programme opens the keynote ‘The many futures of identity and money’ by Rohit Talwar, followed by plenary talks on the first day and then the sessions split into two parallel tracks.

Fall Conference 2019

Charlotte, North Carolina, USA
28–30 October 2019



This year, the Flexographic Technical Association has designed the programme of its Fall Conference as a flexographic racetrack with eight laps that detail the production of a high-quality sample printed by flexography, complemented by the workforce study findings. It starts with the pre-production meeting and press operator training that implements virtual reality, followed by demonstrations of the optimisation process identifying the best combination of print variables, fingerprinting and application of created compensation curves, process control based on the characterisation run and use of ICC profiles across all prepress devices, and process improvement techniques, up to the final production of samples and examination of the challenging print components.

ICFPE 2019 10th International Conference on Flexible and Printed Electronics

Taipei, Taiwan
23–25 October 2019



The anniversary
10th edition of
this technical

conference features numerous invited speakers across all sessions. Each day is opened by plenary keynotes, which include presentations of the current status of OLED displays by Ching W. Tang, collaborative innovation in electronics manufacturing by Marc Benowitz, new capabilities of flexible electrophoretic display technology by Michael D. McCreary, 3D chip stacking technologies by Teruo Hirayama, and two talks on technology evolution for 5G – by Yujun Li and Jan Vardaman.

The topics of the other invited papers cover tactile sensing electronic skin for wearable and robotic applications, bio-inspired structures and functions for wearable sensors, flexible sensors and wearable patches for healthcare and human-machine interfaces, a holistic approach to inkjet printing of OLED displays, development of power supplies for miniaturised sensor systems using printing technology, applications of photonic curing, human-machine interface in the IoT era, an outlook for 3D structural electronics, and much more. The regular sessions are focused on flexible display and organic devices, optic sensors and flexible electrodes, photovoltaics, organic materials, biosensors, energy, printing electronics, soft electronics, measurement and inspection, manufacturing equipment, IoT, printing materials and modelling.

ERA Packaging & Decorative Conference 2019



Kiel, Germany
6–7 November 2019

This year the conference covers effects of climate policies on the gravure industry, new surfaces for gravure cylinders, seven-colour extended gamut in gravure, etc.

11th Workflow Symposium

Stuttgart, Germany
7 November 2019

In 2019, this free-of-charge symposium on Job Definition



Format, Industry 4.0 and workflow automation offers presentations discussing the work of ISO and CIP4 organisations, including the Print Procurement Workgroup of the latter, dealing with the standardisation of automated interactions in online printing and development of the corresponding ICS (Interoperability Conformance Specification) to facilitate the use of PrintTalk and XJDF, along with the examples of commercial workflow solutions, their practical implementations, efficient project planning and possible benefits of XJDF in quality monitoring.

Grafkom Nordic Workflow Summit 2019

Stockholm, Sweden
12 November 2019 GRAFKOM

Grafkom, a network for the printing industry in the Nordic and Baltic region, hosts the second edition of the Workflow Summit that was successfully launched last year. Besides a keynote by Dietrich von Seggern giving an overview of recent software developments for PDF automation, the summit introduces various workflow solutions and also presents font lifecycle in print and publishing workflows.

World Congress on Active & Intelligent Packaging

Amsterdam, Netherlands
18-19 November 2019

In 2019, a two-day programme of this event



features various examples of smart packaging projects, applications and technology, such as the dynamic QR code data logging or product-specific codes, among others.

ESMA Events



Besides the two conferences introduced below, the European Association of Specialist Printing Manufacturers organises this autumn the workshop on the industrial digital printing, prepared again in cooperation with Fraunhofer IPA and Hochschule der Medien. The 2019 edition is intended for the German-speaking participants and takes place from 2 to 5 December in Stuttgart, Germany.

TheIJC 2019

The 6th European Edition of The Inkjet Conference



Düsseldorf, Germany
29-30 October 2019

Keeping the successful format, both days of The Inkjet Conference start with plenary sessions and continue with sessions in three programme tracks. All plenary talks of this edition are about printheads. The topics announced so far include a modular approach to allow quick building of application-specific print systems, available options in providing colour consistency, tests on jetting directions, jetting distances from the printhead to the substrate and jettable fluid parameters, modelling key performance parameters for inkjet printhead design, new printheads utilising an improved piezoelectric ceramic actuator or other component and design enhancements, and the compact-sized recirculation system. About one-third of the lectures in split tracks present various advanced inkjet applications and related research, such as the study of flow-induced damage and chemistry within printing flow systems. Numerous talks deal also with ink formulation and ink components, as well as with various characterisation methods. Developments in the areas of UV curing, IR drying, software and hardware are also covered.

GlassPrint 2019



Düsseldorf, Germany
27-28 November 2019

This year's programme of the conference covering digital and screen printing technologies for decorating glass features the keynotes presenting the container glass industry vision (by Michael Delle Selve) and possible energy savings and CO₂ emission reduction (by Luca Oggianu), as well as the keynotes on the German glass industry and the status of Glasstec 2020. The technical lectures explore the adhesion of UV-curable inkjet inks on glass, CtP technologies for screen printing and pad printing, suitable automation solutions, sol-gel inkjet printing for transparent conductors, and more.

Paper & Beyond

Brussels, Belgium
18-19 November 2019



The main focus of this event organised by the Confederation of European Paper Industries is on paper industry contribution to EU 2050 climate neutrality. The sessions also bring the vision and agenda for forest-based industries towards 2050, topical panel discussions, and the Blue Sky Young Researchers & Innovation Award.

Call for papers

The Journal of Print and Media Technology Research is a peer-reviewed periodical, published quarterly by **iarigai**, the International Association of Research Organizations for the Information, Media and Graphic Arts Industries.

JPMTR is listed in Emerging Sources Citation Index, Scopus, Index Copernicus International, PiraBase (by Smithers Pira), Paperbase (by Innventia and Centre Technique du Papier), NSD – Norwegian Register for Scientific Journals, Series and Publishers.

Authors are invited to prepare and submit complete, previously unpublished and original works, which are not under review in any other journals and/or conferences.

The journal will consider for publication papers on fundamental and applied aspects of at least, but not limited to, the following topics:

- ⊕ **Printing technology and related processes**
Conventional and special printing; Packaging; Fuel cells, batteries, sensors and other printed functionality; Printing on biomaterials; Textile and fabric printing; Printed decorations; 3D printing; Material science; Process control
- ⊕ **Premedia technology and processes**
Colour reproduction and colour management; Image and reproduction quality; Image carriers (physical and virtual); Workflow and management
- ⊕ **Emerging media and future trends**
Media industry developments; Developing media communications value systems; Online and mobile media development; Cross-media publishing
- ⊕ **Social impact**
Environmental issues and sustainability; Consumer perception and media use; Social trends and their impact on media

Submissions for the journal are accepted at any time. If meeting the general criteria and ethic standards of scientific publishing, they will be rapidly forwarded to peer-review by experts of relevant scientific competence, carefully evaluated, selected and edited. Once accepted and edited, the papers will be published as soon as possible.

There is no entry or publishing fee for authors. Authors of accepted contributions will be asked to sign a copyright transfer agreement.

Authors are asked to strictly follow the guidelines for preparation of a paper (see the abbreviated version on inside back cover of the journal).

Complete guidelines can be downloaded from: <http://www.iarigai.org/publications/journals/>
Papers not complying with the guidelines will be returned to authors for revision.

Submissions and queries should be directed to: journal@iarigai.org



Vol. 8, 2019

Prices and subscriptions

Since 2016, the journal is published in digital form.
A print version is available on-demand and at additional price.

Please, find below the prices charged for the Journal, as well as for a single paper.
Use the opportunity to benefit from the Subscriber's discount price.

By ordering a publication, or by subscription, a password will be provided to you for downloading.
The password protection of every issue is active during a period of six months.
After this period the publications will be available free of charge.

iarigai members will be given the download password for free.

Regular prices

Four issues, digital JPMTR (password protected)	300 EUR
Single issue, digital JPMTR (password protected)	100 EUR
Single paper from JPMTR (PDF file)	20 EUR
Four issues, print JPMTR (on-demand)	400 EUR
Single issue, print JPMTR (on-demand)	100 EUR

Subscription prices

Annual subscription, four issues, digital JPMTR (password protected)	240 EUR
Annual subscription, four issues, print JPMTR (on-demand)	400 EUR

Prices for **iarigai** members

Four issues, digital JPMTR (password protected)	Free of charge
Single paper from JPMTR (PDF file)	Free of charge
Four issues, print JPMTR (on-demand)	400 EUR
Single issue, print JPMTR (on-demand)	100 EUR

Place your order online at: <http://www.iarigai.org/publications/subscriptions-orders/>
Or send an e-mail order to: office@iarigai.org

Guidelines for authors

Authors are encouraged to submit complete, original and previously unpublished scientific or technical research works, which are not under reviews in any other journals and/or conferences. Significantly expanded and updated versions of conference presentations may also be considered for publication. In addition, the Journal will publish reviews as well as opinions and reflections in a special section.

Submissions for the journal are accepted at any time. If meeting the general criteria and ethical standards of the scientific publication, they will be rapidly forwarded to peer-review by experts of high scientific competence, carefully evaluated, and considered for selection. Once accepted by the Editorial Board, the papers will be edited and published as soon as possible.

When preparing a manuscript for JPMTR, please strictly comply with the journal guidelines. The Editorial Board retains the right to reject without comment or explanation manuscripts that are not prepared in accordance with these guidelines and/or if the appropriate level required for scientific publishing cannot be attained.

A – General

The text should be cohesive, logically organized, and thus easy to follow by someone with common knowledge in the field. Do not include information that is not relevant to your research question(s) stated in the introduction.

Only contributions submitted in English will be considered for publication. If English is not your native language, please arrange for the text to be reviewed by a technical editor with skills in English and scientific communications. Maintain a consistent style with regard to spelling (either UK or US English, but never both), punctuation, nomenclature, symbols etc. Make sure that you are using proper English scientific terms. Literal translations are often wrong. Terms that do not have a commonly known English translation should be explicitly defined in the manuscript. Acronyms and abbreviations used must also be explicitly defined. Generally, sentences should not be very long and their structure should be relatively simple, with the subject located close to its verb. Do not overuse passive constructions.

Do not copy substantial parts of your previous publications and do not submit the same manuscript to more than one journal at a time. Clearly distinguish your original results and ideas from those of other authors and from your earlier publications – provide citations whenever relevant.

For more details on ethics in scientific publication consult Guidelines, published by the Committee on Publication Ethics (COPE): <https://publicationethics.org/resources/guidelines>

If it is necessary to use an illustration, diagram, etc. from an earlier publication, it is the author's responsibility to ensure that permission to reproduce such an illustration, diagram, etc. is obtained from the copyright holder. If a figure is copied, adapted or redrawn, the original source must be acknowledged.

Submitting the contribution to JPMTR, the author(s) confirm that it has not been published previously, that it is not under consideration for publication elsewhere and – once accepted and published – it will not be published under the same title and in the same form, in English or in any other language. The published paper may, however, be republished as part of an academic thesis to be defended by the author. The publisher retains the right to publish the printed paper online in the electronic form and to distribute and market the Journal containing the respective paper without any limitations.

B – Structure of the manuscript Preliminary

Title: Should be concise and unambiguous, and must reflect the contents of the article. Information given in the title does not need to be repeated in the abstract (as they are always published jointly), although some overlap is unavoidable.

List of authors: I.e. all persons who contributed substantially to study planning, experimental work, data collection or interpretation of results and wrote or critically revised the manuscript and approved its final version. Enter full names (first and last), followed by the present address, as well as the E-mail addresses. Separately enter complete details of the corresponding author – full mailing address, telephone number, and E-mail. Editors will communicate only with the corresponding author.

Abstract: Should not exceed 500 words. Briefly explain why you conducted the research (background), what question(s) you answer (objectives), how you performed the research (methods), what you found (results: major data, relationships), and your interpretation and main consequences of your findings (discussion, conclusions). The abstract must reflect the content of the article, including all keywords, as for most readers it will be the major source of information about your research. Make sure that all the information given in the abstract also appears in the main body of the article.

Keywords: Include three to five relevant scientific terms that are not mentioned in the title. Keep the keywords specific. Avoid more general and/or descriptive terms, unless your research has strong interdisciplinary significance.

Scientific content

Introduction and background: Explain why it was necessary to carry out the research and the specific research question(s) you will answer. Start from more general issues and gradually focus on your research question(s). Describe relevant earlier research in the area and how your work is related to this.

Methods: Describe in detail how the research was carried out (e.g. study area, data collection, criteria, origin of analyzed material, sample size, number of measurements, equipment, data analysis, statistical methods and software used). All factors that could have affected the results need to be considered. Make sure that you comply with the ethical standards, with respect to the environmental protection, other authors and their published works, etc.

Results: Present the new results of your research (previously published data should not be included in this section). All tables and figures must be mentioned in the main body of the article, in the order in which they appear. Make sure that the statistical analysis is appropriate. Do not fabricate or distort any data, and do not exclude any important data; similarly, do not manipulate images to make a false impression on readers.

Discussion: Answer your research questions (stated at the end of the introduction) and compare your new results with published data, as objectively as possible. Discuss their limitations and highlight your main findings. At the end of Discussion or in a separate section, emphasize your major conclusions, pointing out scientific contribution and the practical significance of your study.

Conclusions: The main conclusions emerging from the study should be briefly presented or listed in this section, with the reference to the aims of the research and/or questions mentioned in the Introduction and elaborated in the Discussion.

Note: Some papers might require different structure of the scientific content. In such cases, however, it is necessary to clearly name and mark the appropriate sections, or to consult the editors. Sections from Introduction until the end of Conclusions must be numbered. Number the section titles consecutively as 1., 2., 3., ... while subsections should be hierarchically numbered as 2.1, 2.3, 3.4 etc. Only Arabic numerals will be accepted.

Acknowledgments: Place any acknowledgements at the end of your manuscript, after conclusions and before the list of literature references.

References: The list of sources referred to in the text should be collected in alphabetical order on at the end of the paper. Make sure that you have provided sources for all important information extracted from other publications. References should be given only to documents which any reader can reasonably be expected to be able to find in the open literature or on the web, and the reference should be complete, so that it is possible for the reader to locate the source without difficulty. The number of cited works should not be excessive - do not give many similar examples.

Responsibility for the accuracy of bibliographic citations lies entirely with the authors. Please use exclusively the Harvard Referencing System. For more information consult the Guide to Harvard style of Referencing, 6th edition, 2019, used with consent of Anglia Ruskin University, available at: https://libweb.anglia.ac.uk/referencing/files/Harvard_referencing_201718.pdf

C – Technical requirements for text processing

For technical requirement related to your submission, i.e. page layout, formatting of the text, as well of graphic objects (images, charts, tables etc.) please see detailed instructions at:

<http://www.iarigai.org/publications/journals/>

D – Submission of the paper and further procedure

Before sending your paper, check once again that it corresponds to the requirements explicated above, with special regard to the ethical issues, structure of the paper as well as formatting.

Once completed, send your paper as an attachment to: journal@iarigai.org

If necessary, compress the file before sending it. You will be acknowledged on the receipt within 48 hours, along with the code under which your submission will be processed.

The editors will check the manuscript and inform you whether it has to be updated regarding the structure and formatting. The corrected manuscript is expected within 15 days.

Your paper will be forwarded for anonymous evaluation by two experts of international reputation in your specific field. Their comments and remarks will be in due time disclosed to the author(s), with the request for changes, explanations or corrections (if any) as demanded by the referees.

After the updated version is approved by the reviewers, the Editorial Board will decide on the publishing of the paper. However, the Board retains the right to ask for a third independent opinion, or to definitely reject the contribution.

Printing and publishing of papers, once accepted by the Editorial Board, will be carried out at the earliest possible convenience.

3-2019

Journal of Print and Media Technology Research

A PEER-REVIEWED QUARTERLY

The journal is publishing contributions
in the following fields of research

- ⊕ Printing technology and related processes
- ⊕ Premedia technology and processes
- ⊕ Emerging media and future trends
- ⊕ Social impacts

For details see the Mission statement inside

JPMTR is listed in

- ⊕ Emerging Sources Citation Index
- ⊕ Scopus
- ⊕ Index Copernicus International
- ⊕ PiraBase (by Smithers Pira)
- ⊕ Paperbase (by Innventia and Centre Technique du Papier)
- ⊕ NSD – Norwegian Register for Scientific Journals, Series and Publishers

Submissions and inquiries

journal@iarigai.org

Subscriptions

office@iarigai.org

More information at

www.iarigai.org/publications/journal



Publisher

The International Association of Research Organizations
for the Information, Media and Graphic Arts Industries
Magdalenenstrasse 2
D-64288 Darmstadt
Germany

